MTL TR 89-42

AD

AD-A212 095

(2)

DEFORMATION BEHAVIOR OF SiC/2014 Al METAL-MATRIX COMPOSITE

SHUN-CHIN CHOU, DATTATRAYA P. DANDEKAR, JOHN L. GREEN, ANTHONY G. MARTIN, and RONALD A. SWANSON
U.S. ARMY MATERIALS TECHNOLOGY LABORATORY
MATERIALS DYNAMICS BRANCH

JULIUS FRANKEL
BENET WEAPONS LABORATORY, WATERVLIET, NY

JIBMITRA GANGULY
UNIVERSITY OF ARIZONA, TUCSON, AZ

CRAIG LOPATIN
UNIVERSITY OF DAYTON RESEARCH INSTITUTE, DAYTON, OH

May 1989

Approved for public release; distribution unlimited.

US ARMY
LABORATORY COMMAND
MATERIALS TECHNOLOGY LABORATORY

U.S. ARMY MATERIALS TECHNOLOGY LABORATORY
Watertown, Massachusetts 02172-0001

UNCLASSIFIED

SECURITY CLASSIFICATION OF THIS PAGE (When Data Entered)

REPORT DOCUMENTATION PAGE

READ INSTRUCTIONS BEFORE COMPLETING FORM

1. REPORT NUMBER: MTL TR 89-42	2. GOVT ACCESSION NO.
3. RECIPIENT'S CATALOG NUMBER	
4. TITLE (and Subtitle): DEFORMATION BEHAVIOR OF SiC/2014 Al METAL-MATRIX COMPOSITE	5. TYPE OF REPORT & PERIOD COVERED: Final Report
	6. PERFORMING ORG. REPORT NUMBER
7. AUTHOR(s): Shun-Chin Chou, Dattatraya P. Dandekar, Julius Frankel,* Jibmitra Ganguly,† John L. Green, Craig Lopatin,‡ Anthony G. Martin, and Ronald A. Swanson	8. CONTRACT OR GRANT NUMBER(s)
9. PERFORMING ORGANIZATION NAME AND ADDRESS: U.S. Army Materials Technology Laboratory, Watertown, Massachusetts 02172-0001, SLCMT-MRD	10. PROGRAM ELEMENT, PROJECT, TASK AREA & WORK UNIT NUMBERS: D/A Project: 536-6010 P623222.K14A-2585 AMCMS Code: 69200R.897 A050
11. CONTROLLING OFFICE NAME AND ADDRESS: U.S. Army Laboratory Command, 2800 Powder Mill Road, Adelphi, Maryland 20783-1145	12. REPORT DATE: May 1989
	13. NUMBER OF PAGES: 46
14. MONITORING AGENCY NAME & ADDRESS (if different from Controlling Office)	15. SECURITY CLASS. (of this report): Unclassified
	15a. DECLASSIFICATION/DOWNGRADING SCHEDULE

16. DISTRIBUTION STATEMENT (of this Report)

Approved for public release; distribution unlimited.

17. DISTRIBUTION STATEMENT (of the abstract entered in Block 20, if different from Report)

18. SUPPLEMENTARY NOTES

*U.S. Army Armament Research and Development Command, Benet Weapons Laboratory, Watervliet, NY 12183

†University of Arizona, Tucson, AZ 85721

‡University of Dayton Research Institute, Dayton, OH 45469

19. KEY WORDS (Continue on reverse side if necessary and identify by block number)

Elastic constants	Strain rate	Deformation
High temperature	Fracture toughness	Bauschinger effect
Spallation	Shock loading	Composite materials
Metal-matrix composites	Equation of state	

20. ABSTRACT (Continue on reverse side if necessary and identify by block number)

(SEE REVERSE SIDE)

DD FORM 1 JAN 73 1473 EDITION OF 1 NOV 65 IS OBSOLETE

UNCLASSIFIED

SECURITY CLASSIFICATION OF THIS PAGE (When Data Entered)

Block No. 20

ABSTRACT

The deformation behavior of a composite composed of 25-volume-percent silicon carbide (SiC) whiskers in 2014 aluminum matrix was studied. Specimens were taken from a hot isostatically pressed cylindrical billet, then tested at various loading conditions and strain rates. Mechanical deformation of the composite was performed using tension, compression, torsion, Bauschinger effect, and fracture toughness testing. Deformation of the composite under shock loading/unloading and spallation threshold were determined. Elastic wave velocities at high pressures to 1.5 GPa and volume compression to 4.5 GPa were measured to determine the pressure dependence of elastic constants and isothermal and adiabatic equations of state.

CONTENTS

Page

INTRODUCTION . . . 1

MATERIALS DESCRIPTION . . . 1

MECHANICAL DEFORMATION AT STRAIN RATES TO 5 sec^{-1}

Introduction . . . 3
Room Temperature Experiments . . . 3
Test Results and Discussion . . . 6
High Heating Rate - High Temperature Experiments . . . 12
Summary . . . 20

PRESSURE DEPENDENCE OF THE ELASTIC CONSTANTS

Introduction . . . 22
Specimens and Ultrasonic Technique . . . 22
Results of Ultrasonic Experiments . . . 24
Elastic Constants at the Ambient Condition . . . 24
Elastic Constants at Elevated Pressures . . . 25
Discussion . . . 29
Conclusions . . . 31

COMPRESSION AT HIGH PRESSURES

Introduction . . . 31
Specimen and Experimental Detail . . . 32
Calculation of Volume Change . . . 34
Discussion . . . 36
Conclusions . . . 37

SHOCK RESPONSE

Introduction . . . 37
Specimen and Experimental Details . . . 37
Results . . . 38

SUMMARY

Density . . . 40
Elastic Constants . . . 40
Limits of Elastic Deformation, Ductility, and Strength . . . 41
Equation of State . . . 42
Shock Deformation . . . 42

REFERENCES . . . 43

INTRODUCTION

The relative advantages of metal-matrix composites over competing materials, like metals and their alloys, depend upon specific application. For example, in application of developing low cost metal-matrix composites for manufacture of interceptor parts to replace monolithic materials like aluminum, titanium, and steel, it is essential that the developed composites possess better mechanical and physical properties compared to the monolithic materials. Some of the critical properties for this application are higher stiffness, higher strength, controlled thermal expansion coefficient, better elevated temperature and pressure properties, better fracture toughness, higher spall threshold, augmented damping, etc. One of the candidate metal-matrix composites identified for such application was silicon carbide whisker-reinforced aluminum matrix. The specific metal-matrix composite chosen for the present investigation was silicon carbide whisker-reinforced (25% by volume) 2014 aluminum alloy. The composite properties investigated are:

1. mechanical deformation under uniaxial stress at 10^{-4} and 5 sec^{-1} at room temperature,

2. mechanical deformation under uniaxial stress at a strain rate of 5 sec^{-1} at elevated temperatures and at different heating rates,

3. Bauschinger effect by precompressing to two different strain levels at room temperature,

4. fracture toughness at room temperature,

5. mechanical deformation under torsion,

6. elastic wave velocities at high pressures to 1.5 GPa,

7. volume compression to 4.5 GPa,

8. deformation under shock loading (strain rate of 10^6 sec^{-1}) and unloading, and

9. spallation threshold.

The structure of the report is as follows: The Materials Description Section gives a brief description of the composite; the deformation behavior of the composite under medium strain rates, i.e., 5 sec^{-1} and various loading conditions, are described in the Mechanical Deformation at Strain Rates to 5 sec^{-1} Section; the Pressure Dependence of the Elastic Constants Section and the Compression at High Pressures Section deal with the pressure dependence of elastic constants and isothermal and adiabatic equations of state, respectively; the Shock Response Section deals with the deformation of the composite under shock loading, i.e., under impact loading and its spall threshold; and the Summary Section provides a general summary of the results given in the previous four sections.

MATERIALS DESCRIPTION

The silicon carbide aluminum composite used in the present work consists of randomly dispersed 25-volume-percent silicon carbide whiskers in a 2014 aluminum alloy matrix. The whiskers were 0.2 to 0.5 micron in diameter and had a length-to-diameter ratio of

approximately 80. Billets of the above mentioned compositions were fabricated by the hot isostatic press (HIP) method. The HIPed material was subsequently given the conventional heat treatment bringing 2014 aluminum to the T4 condition. For 2014 aluminum alloy, T4 condition involves: (1) heating the alloy to 769 ± 6°K, (2) keeping it at this temperature for 1 to 2 hours, (3) quenching the alloy in water, and (4) aging the alloy at room temperature. This treatment basically homogenizes the material and tends to eradicate most of the detrimental microstructural variations in 2014 aluminum alloy. The above treatment was given to the present composite material (SiC/2014-T4 Al) under the hypothesis that it would reduce the variations in the material properties in or among the billets. The billets of SiC/2014-T4 Al obtained in the above manner were in the form of thick-walled cylinders. The specimens of SiC/2014-T4 Al were obtained so as to have their faces either normal to the axis of the cylindrical billets (z axis SiC) or normal to the radial direction (r) of the cylindrical billets. The specimens of SiC/2014-T4 Al with face normal in z and r directions are identified, respectively, as SiC/Al (z) and SiC/Al (r) in this report. Figure 1 shows a photomicrograph of SiC/Al (z) and SiC/Al (r) specimens. It shows that the whiskers are randomly oriented in the aluminum matrix. As a consequence, mechanical properties were expected to be isotropic.

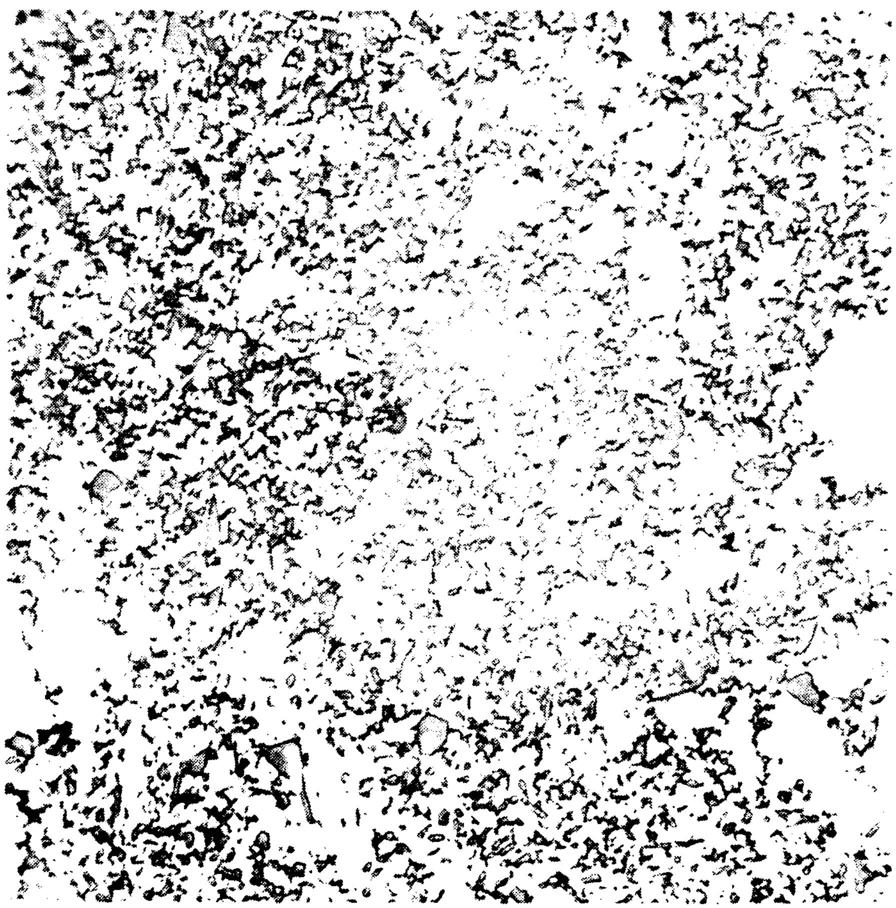

Figure 1. Photomicrograph of SiC/2014-T4 aluminum.

The average density of SiC/2014-T4 Al was determined to be 2.91 $\pm$ 0.01 Mg/m^3; the expected theoretical density of the composite. The average values of the longitudinal and shear elastic wave velocities determined by ultrasonic technique were 7.31 $\pm$ 0.03 km/sec and 3.89 $\pm$ 0.01 km/sec, respectively. These measurements were performed on nine different specimens of SiC/Al (z) and SiC/Al (r) [Table 1]. These results show that as received SiC/Al is isotropic with respect to its elastic properties. They are discussed further in the Pressure Dependence of the Elastic Constants Section.

Table 1. PHYSICAL PROPERTIES OF SiC/2014-T4 ALUMINUM AS A FUNCTION OF ORIENTATION OF SPECIMENS

	Orientation*		
Physical Properties	Z	R	Small Specimen
Density (Mg/m^3)	2.908 ± 0.028	2.904 ± 0.006	2.906
Density Range (Mg/m^3)	2.890 - 2.915	2.900 - 2.907	
Elastic Velocity (km/sec)			
Longitudinal	7.284 ± 0.050	7.329 ± 0.02	7.381 ± 0.015
Shear (1)	3.870 ± 0.02	3.866 ± 0.010	3.902 ± 0.008
Shear (2)	3.885 ± 0.02	3.918 ± 0.014	

*These values represent an average of measurements performed on nine different specimens of each orientation

MECHANICAL DEFORMATION AT STRAIN RATES TO 5 sec^{-1}

Introduction

In this section, attention is focused on the deformation behavior of the SiC/2014-T4 Al composite when subjected to various stress conditions at strain rates ranging from quasistatic to 5 sec^{-1}. In addition, its deformation behavior was investigated at high heating rates of 14°C/sec to 250°C/sec with temperature reaching 540°C at a strain rate of 5 sec^{-1}. The results of this section provide necessary design data to evaluate suitability of SiC/2014-T4 Al composite for specific applications.

Room Temperature Experiments

Specimens of SiC/Al were tested in tension, compression, and torsion. The Bauschinger effect was investigated by precompressing specimens to a prescribed strain level, then reversing the load direction to tension until specimens fractured. Fracture toughness, K_Q, was measured by using the short rod technique developed by L. M. Barker.[1] The geometry and dimensions of the various test specimens used are shown in Figures 2 through 6.

The test conditions in this study were quite diversified. Not only were specimens subjected to various loading conditions, but also to a range of strain rates. Three test apparatus were used to cover all of the test conditions. One of the apparatus is a specially designed test machine incorporated with gage condition units and a fast data acquisition system. The test machine has two operating modes: servo-hydraulic control mode or closed-loop mode, and pneumatic operating mode or open-loop mode. The closed-loop mode covers the range of strain/load/displacement rates from quasistatic to 10^{-1} sec^{-1}, while the open-loop mode

1. BARKER, L. M. *Theory for Determining K_{Ic} from Small Non-LEFM Specimens, Supported by Experiments on Aluminum.* International Journal of Fracture, v. 15, no. 6, December 1979, p. 515-536.

covers the range from approximately 10^{-1} to 50 sec^{-1}, depending on the ductility of the specimen being tested. In the closed-loop mode, the rate can be precisely controlled However, in the open-loop mode, only a nominal rate can be achieved by adjusting the gas pressure, stroke, and size of release orifice in the fast-acting valve. This machine was used to complete the tensile, compression, and Bauschinger effect tests. All specimens were strain gaged, and load and strain were recorded for analysis. Torsion tests were carried out in a standard Instron machine, and torque and twist angle were measured.

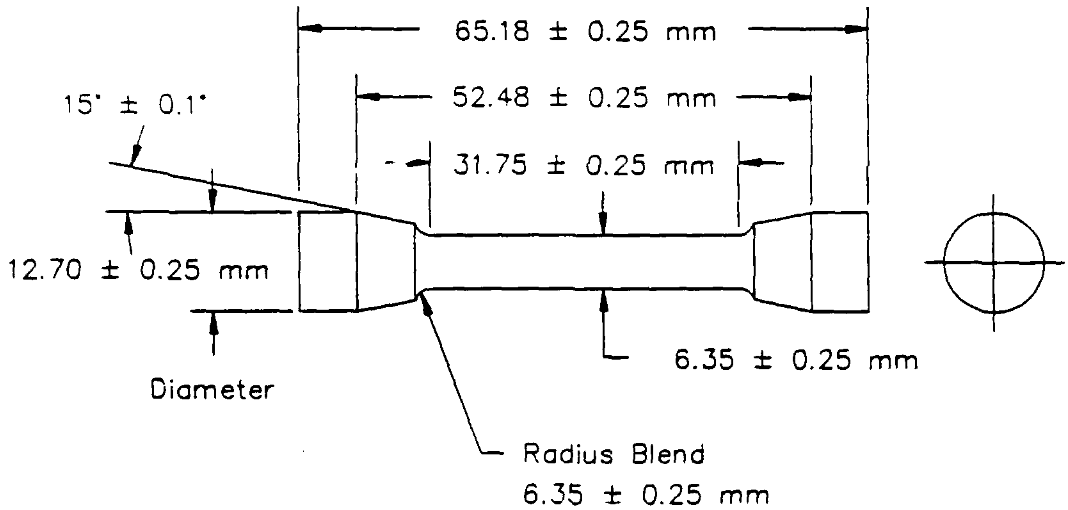

Figure 2. Tension specimen.

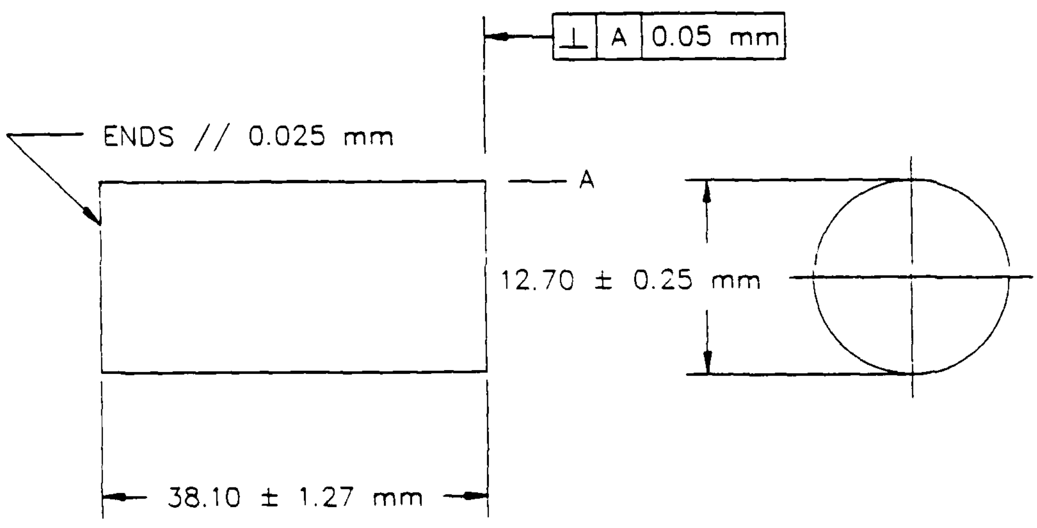

Figure 3. Compression specimen.

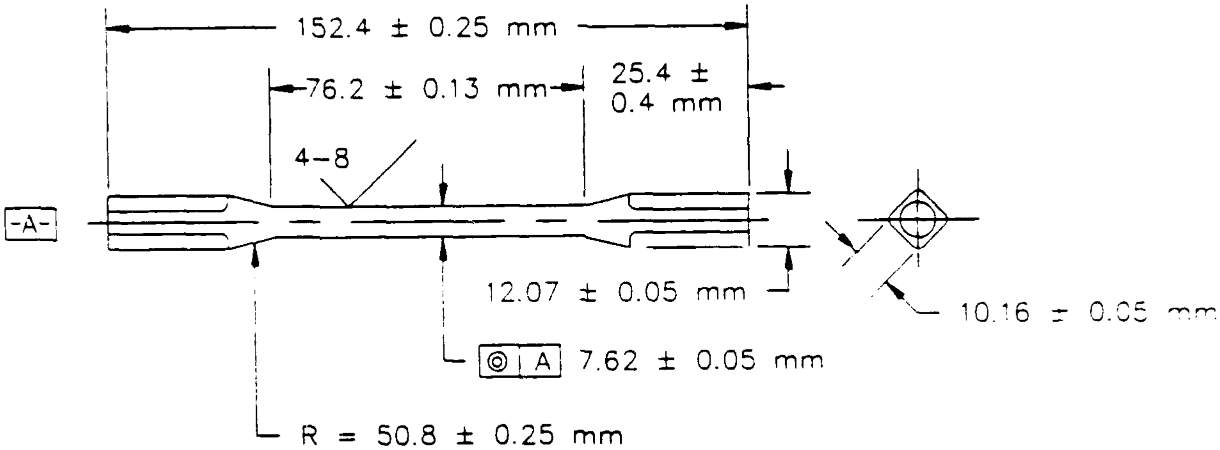

Figure 4. Torsion specimen.

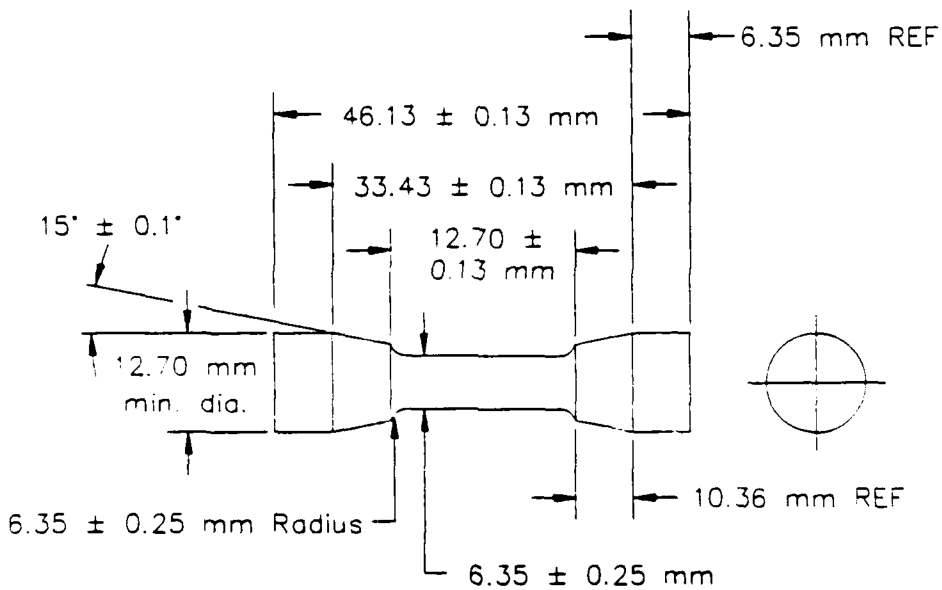

Figure 5. Bauschinger effect specimen.

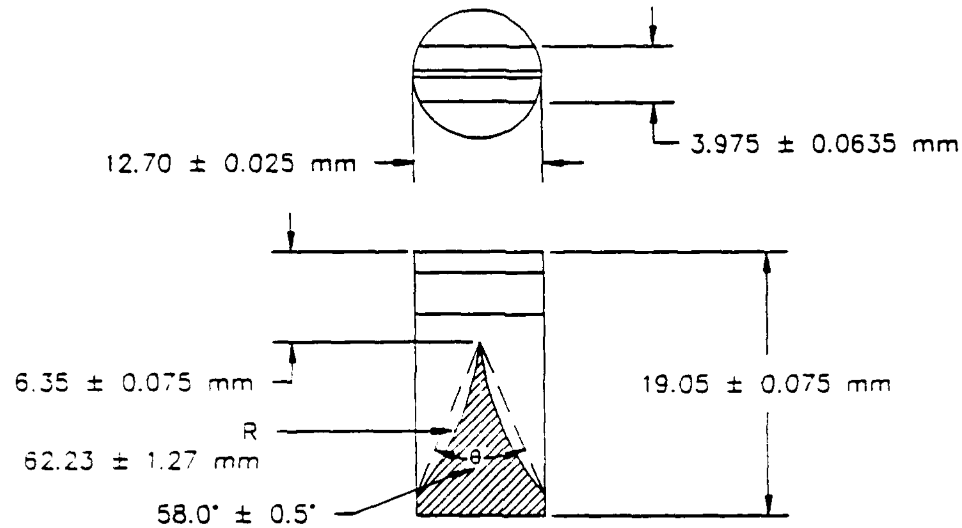

Figure 6. Short rod fracture toughness specimen.

The mode I fracture toughness value, K_Q, was measured with a fractometer manufactured by Terra Tek, Inc. The specimen was a short rod with a length-to-diameter ratio equal to 1.5 (Figure 6). A curved Chevron notch was machined at one end of the specimen, and a fatigue crack was not required before testing. A specially designed set of grips applied the load at the end of the Chevron notch. The load and the displacement at the load points were measured. The K_Q was calculated by following the manufacturer's procedure.[2]

Test Results and Discussion

The metal-matrix composite material SiC/2014 Al was characterized under tension, compression, and torsion. In addition, Bauschinger effect was investigated and fracture toughness value K_{Ic} was determined. The effect of reinforcement with SiC whiskers was investigated by comparing test results of SiC/2014 Al with those of 2014-T4 Al alloy tested at the same conditions. Results from each test condition will be discussed separately in the following sections.

Tension

Tension tests were performed at two strain rates, 10^{-4} and 5 sec^{-1}. Results are shown in Figures 7 and 8 for SiC/2014-T4 Al and 2014-T4 Al, respectively. It is noticed that neither material is strain-rate sensitive for the range of strain rates tested. The average value of elastic modulus for SiC/2014-T4 Al is 120.7 GPa, which is more than 60 percent higher than that for the 2014-T4 Al. Strength data are not presented; the reasons are explained as follows. Tests were performed in the closed-loop mode with strain as a feedback-controlling parameter to ensure a constant strain-rate condition. This constant strain-rate condition was maintained as long as the strain gage on the specimen was functional. If the strain gage failed for some reason before the end of the test, the test machine would be uncontrollable

2. Fractometer System 4202 Owner's Manual. Terra Tek, Inc., Salt Lake City, Utah, 1983.

and the specimen would be fractured in tension immediately. Since the strain, load, and displacement data must be sampled at a rate corresponding to the rate of testing due to the finite number of core memory available in the data acquisition system, the response of the test machine was so rapid after the gage failed, that the specimen was fractured within a sampling interval. Therefore, the last data points were not the ultimate strength and strain; they were the data points just before the gage failure. This explanation was proved to be true by postmortem examination of the specimens, and conducting tensile tests in closed-loop mode with the displacement as a controlling parameter. At this mode, the test results indicated that the ultimate strength of SiC/2014 Al under investigation is consistently higher than 586 MPa.

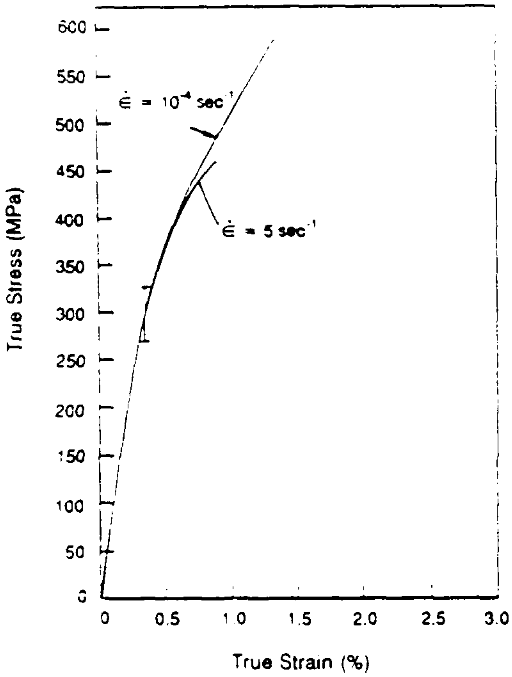

Figure 7. Tension test of SiC/2014-T4 Al at room temperature and strain rates of 10^{-4} and 5 sec^{-1}.

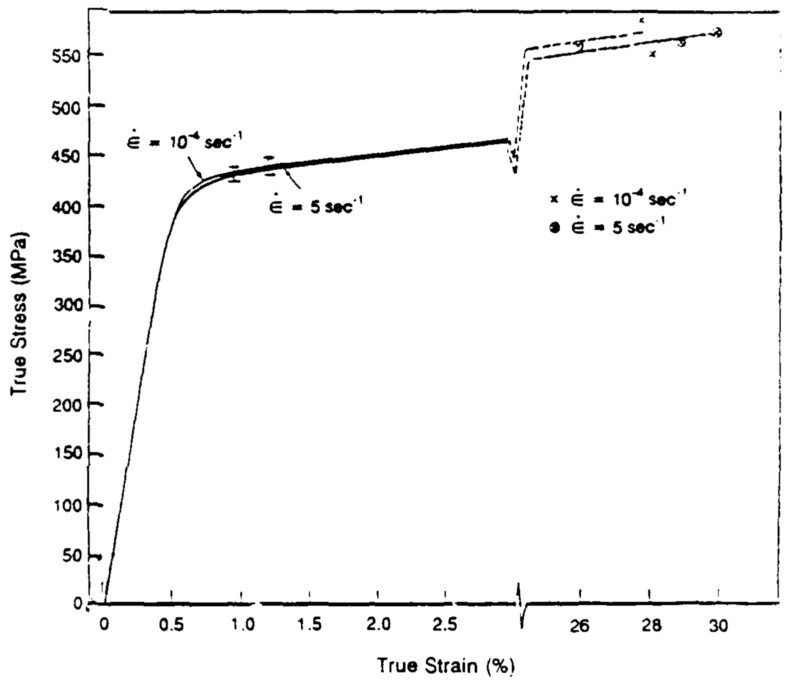

Figure 8. Tension test of 2014-T4 Al at room temperature and strain rates of 10^{-4} and 5 sec^{-1}.

The location of a strain gage on the specimen very often did not coincide with the location of failure. This occurrence will not affect the interpretation of test results for SiC/Al because of the brittle nature of the material. However, the same comment cannot be applied to test results of 2014-T4 Al, which exhibited necking before fracture took place. In this situation, the recorded maximum strain value is not the strain at failure if the strain gage is not at the location where fracture and necking of the specimen take place. A correction was made in the analysis of test results. The diameter of the necked section where fracture occurred was measured after the test, and the ultimate strength was calculated based on the measured necked area rather than the original area. The strain at failure was calculated by assuming that the volume of material remained constant during the plastic deformation which yields the expression for the true strain, e,

$$e = \ln (L/L_0) = \ln(A_0/A) \tag{1}$$

where A_0 and L_0 are original area and length, while A and L are in the deformed state. The stress-strain curves shown in Figure 7 include the interpretation discussed above, and the axes are labeled as "true stress" and "true strain" to reflect this correction.

The tensile results indicate that the whisker reinforcement has increased the modulus by approximately 60 percent and the ultimate strength slightly, but the ductility has been drastically reduced in comparison with those of matrix alloys.

Compression

The compression specimens were machined according to the ASTM standards, with the ratio of length-to-diameter equal to three (Figure 3). Test were performed at two strain rates, 10^{-4} and 5 sec^{-1}, and results are shown in Figure 9. There is no indication of strain-rate sensitivity in the range of interest. The average elastic modulus is about the same as that in tension, 120.7 GPa. Specimens were slightly buckled before failing in shear; i.e., the failure surface had an inclination of about 45° from the direction of the load. The stress levels at failure are indicated by crosses in Figure 9.

Torsion

The torque and twist angle was measured during torsion tests. Results are shown in Figure 10. The initial linear relationship between torque and twist angle can be used to calculate the shear modulus of the specimen. The calculated shear modulus is approximately 44.8 GPa, which, combined with the elastic modulus measured in tensile tests, yields the Poisson's ratio of about 0.3.

The maximum torque may also be estimated by assuming that the material behaves elastic-perfect plastically. The expression for torque is (Ref. 3):

$$M = 2/3\pi \ k \ (a^3 - 1/4 \ c^3) \tag{2}$$

where

M = torque,

k = $Y / \sqrt{3}$ for Von Mises criterion,

a = radius of specimen, and

c = elastic-plastic boundary.

The estimated torque required to cause complete yielding of the specimen (i.e., to set c = 0 and Y = 586 MPa) falls within the range of measured values. This implies that the material is a work-hardening material which is also observed in tensile test results.

3. HILL, R. *The Mathematical Theory of Plasticity.* Oxford University Press, New York, 1950.

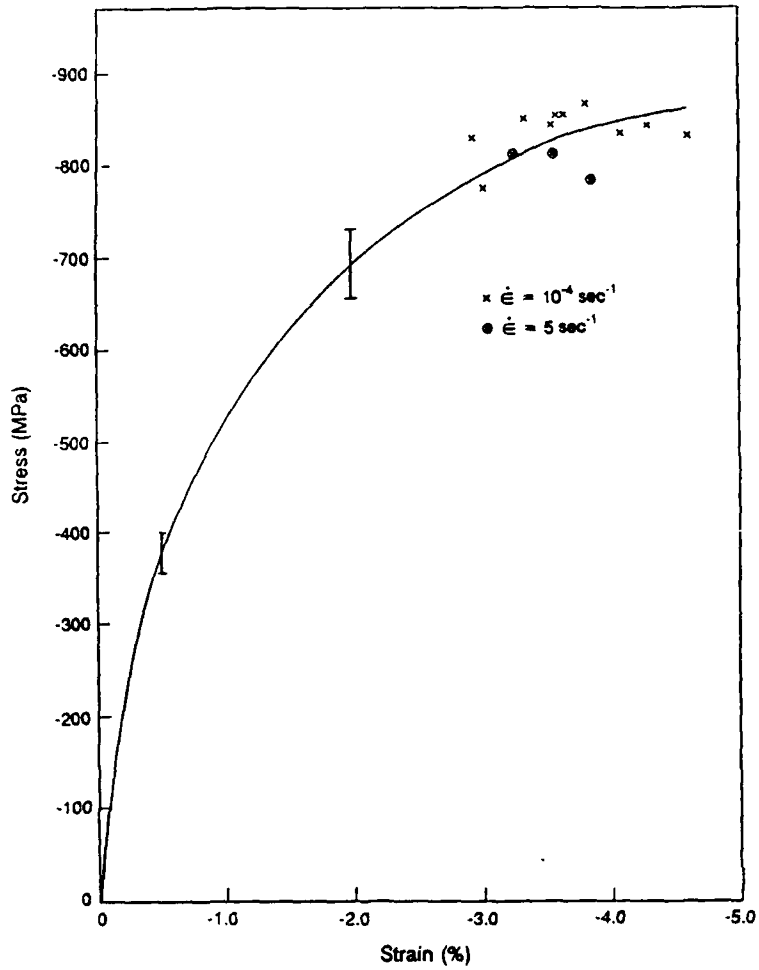

Figure 9. Compression test of SiC/2014-T4 Al at room temperature and strain rates of 10^{-4} and 5 sec^{-1}.

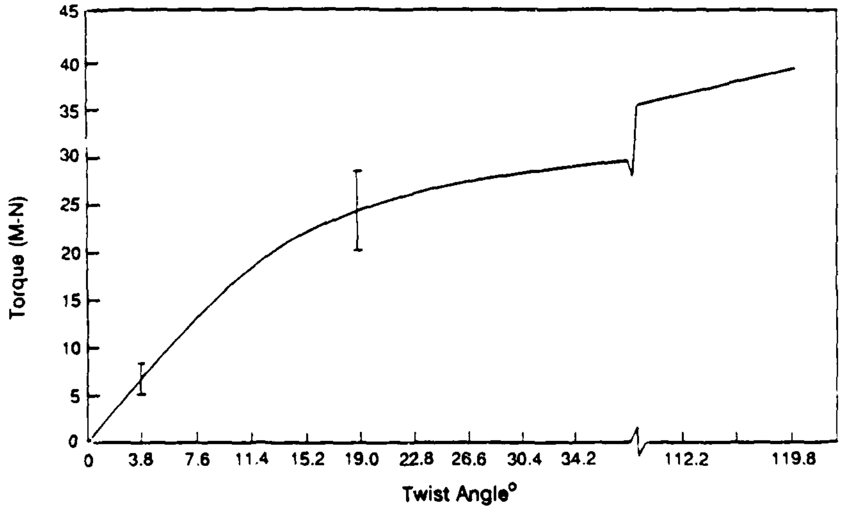

Figure 10. Torsion test result of SiC/2014-T4 Al at room temperature.

Bauschinger Effect

The Bauschinger effect was investigated by precompressing specimens to two strain levels, 1 and 2 percent, then reversing the load direction to tension until specimens fractured. Results are shown in Figures 11 and 12, respectively. It is noticed in Figure 11 that the pre-compression to 1-percent strain seems to have no deteriorating effect on tensile properties such as modulus, ultimate strength, and ductility. The results show that there is approximately 0.5-percent residual strain in the specimen at the completion of unloading. The specimens are stretched to their original length when the tensile stress reaches approximately 310.3 MPa. Finally, the specimens were fractured at stress equal to approximately 586 MPa and strain around 1.5 percent, which are the same as those from the monotonic tension tests.

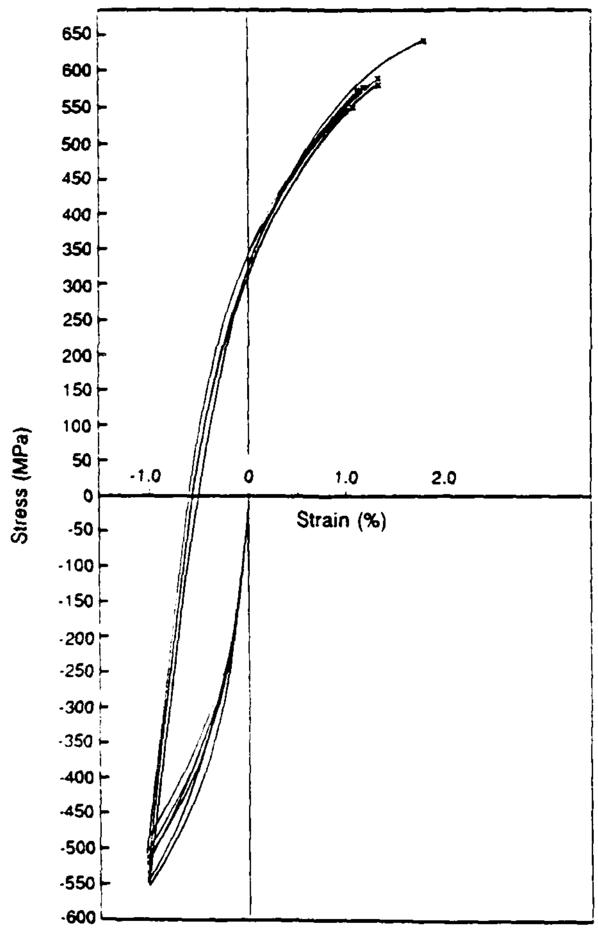

Figure 11. Bauschinger effect test with precompressionto 1-% strain of SiC/2014-T4 Al at room temperature.

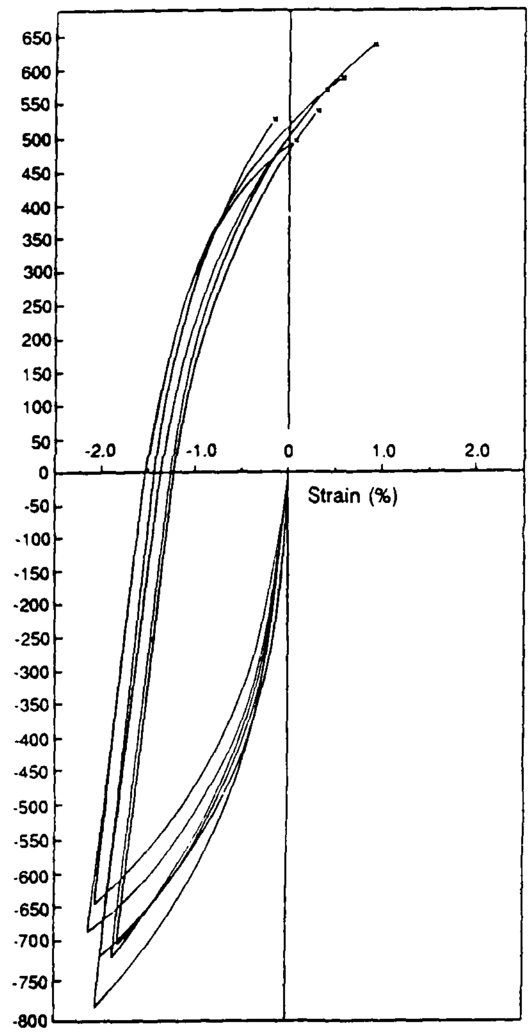

Figure 12. Bauschinger effect test with precompression to 2-% strain of SiC/2014-T4 Al at room temperature.

In the case of specimens precompressed to 2-percent strain (Figure 12), the residual strain at zero stress level is about 1.5 percent. The elastic modulus and ultimate strength seem not to be affected by the precompression; however, the specimens barely return to their original length before fracture.

Based on the results of Bauschinger effect and tensile tests, it seems that the material has a total available tensile strain of approximately 1.5 percent which is not affected by pre-working conditions investigated in this study.

Since there are only limited data available, no attempt to formulate a work-hardening model for this material was made.

Fracture Toughness Measurements

The mode I fracture toughness value, K_{Ic}, was measured by using a Terra Tek Fractometer II testing machine. The specimen was a short rod with a diameter of 1.27 cm and length-to-diameter ratio of 1.5 (Figure 6). The advantage of using this method is that fatigue crack was not needed to ensure the sharpness of the crack tip. K_{Ic} values of many commonly used metals have been measured by using this method, and results agree very well with those obtained by employing a standard ASTM method.

The K_{Ic} value of 2014-T6 Al rolled rod was measured, which agrees very well with the value listed in Ref. 4. It is known that the mechanical behavior of 2014-T4 and T6 alloys are very similar. Hence, the measured 2014-T6 fracture toughness may be used to compare with those of SiC/2014 Al to demonstrate the effect of whisker reinforcement. Table 2 shows the measured K_{Ic} values for both 2014-T6 alloy and SiC/2014 Al composite. The first character in the orientation indicated the load direction, and the second character indicated the direction of crack propagation. The average value of K_{Ic} for 2014-T6 Al is 19.3 MPa $\sqrt{m}$, which agrees with the handbook value.[4] The average value of K_{Ic} for SiC/Al in the Z-R orientation is 13.7 MPa $\sqrt{m}$, while the K_{Ic} in R-Z orientation is 13.3 MPa $\sqrt{m}$.

Table 2. SiC/Al AND 2014-T6 Al FRACTURE TOUGHNESS TEST RESULTS

Material	Spec. No.	Diameter (mm)	Orientation	K_{Ic} SR MPa $\sqrt{m}$	Test Temp. (°C)	R.H. (%)
SiC/Al	R-1	12.726	Z-R	13.1	22.2	50.0
	R-2	12.713	Z-R	14.4		
	R-3	12.703	Z-R	13.1		
	R-4	12.713	Z-R	14.0		
	R-5	12.700	Z-R	14.0		
SiC/Al	Z-1	12.713	R-Z	12.0		
	Z-2	12.713	R-Z	12.7		
	Z-3	12.687	R-Z	13.8		
	Z-4	12.662	R-Z	14.5		
	Z-5	12.680	R-Z	13.3		
2014-T6 Al	L-1	12.700	R-L	19.6		
	L-2	12.700	R-L	19.1		
	L-3	12.687	R-L	19.1		
	L-4	12.700	R-L	19.2		
	L-5	12.700	R-L	19.7	22.2	50.0

Note: Terra Tek Fractometer II testing machine was used to obtain fracture toughness values. Specimen type used was the short rod with curved Chevron slot.

4. MIL-HDBK-5D. *Typical Values of Room Temperature Plane-Strain Fracture Toughness of Aluminum Alloys.* 1 June 1983, p. 3-11.

This is further evidence indicating that the HIP process produces an isotropic material. The low value of K_{Ic} for SiC/Al indicates the brittle behavior of the material which is consistent with the low ductility exhibited in tensile tests.

High Heating Rate - High Temperature Experiments

In these experiments, specimens of SiC/2014-T4 Al were tested in tension and at a strain rate of 5 sec^{-1} only. The geometry and dimensions of these specimens are shown in Figure 13.

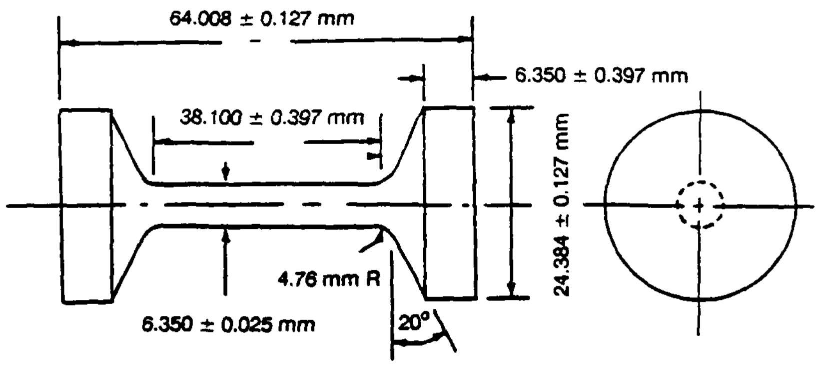

Figure 13. Dimensions of test specimens.

Experimental Setup

The heating apparatus utilizes the resistance heating technique. This method involves passing current through the specimen, using the specimen's resistance to convert the current to heat. The apparatus consists of an autotransformer which is used to control the power output of the apparatus, a step down transformer for converting low current high voltage to high current low voltage, and a high voltage relay which is located between the autotransformer and computer. The system is actuated by a command in the test program to trigger the relay and allow the current to flow to the specimen. Specimen heating rate is proportional to the energy dissipation rate. Assuming an ideal situation in which all energy is converted to heat, the heating rate may be estimated by

$$AMS\,\frac{\Delta T}{\Delta t} = \frac{V2}{R} \tag{3}$$

where A is a conversion factor, M is the mass of the specimen, S is the specific heat of the specimen, T is the temperature, t is the time, V is the applied voltage to the specimen, and R is the resistance of the specimen.

Since no real system is an ideal one, the estimated heating rate just provides a starting point from which the desired heating rate for a particular specimen geometry and material can be obtained by adjusting the voltage and measuring the temperature and time history with an appropriate thermocouple attached to the specimen. The setting on the autotransformer is then used on all subsequent tests for the particular heating rate.

Because alternating current is passed through specimens, the possibility of skin effects must be examined. Skin effects occur when current is alternating, and there are internal effects which tend to force the current to flow mostly in the outer portion of the conductor.[5] The equation which determines the diameter thickness beyond which the skin effect is significant, is

$$\delta = 1/\sqrt{F\mu\sigma\pi} \tag{4}$$

where δ is the thickness of conductor (cm), σ is the conductivity (ohm-cm)$^{-1}$, μ is the permeability (Henry per meter) and F is the frequency (Hz). For aluminum, the conductivity is 0.35×10^6 (ohms-cm)$^{-1}$. The values of M and F are 1.26×10^{-6} H/m and 60 Hz, respectively.

Thus, the value of diameter at which skin effects must be considered is greater than the specimen's diameter (0.635 cm). This ensures that the specimen has a uniform temperature in the gage section. It is assumed that this conclusion is also applicable to SiC/Al specimens.

Special attention must be paid to the design of the grip system because it requires being isolated electrically from the specimen and must be strong enough to sustain the load. Tapered aluminum oxide inserts were used to transmit load and provide insulation both thermally and electrically. The complete grip assembly is shown in Figure 14. The inserts are machined to fit into split-collar bushings and conform to the specimen's geometry. The specimen is inserted into the split collars first, before the two split collars are assembled and threaded into the top and bottom cylindrical couplers. Copper electrodes are used as conductors, which are spring loaded to maintain contact with both ends of the specimen at all times. Copper electrodes and springs are insulated from the cylindrical couplers with nylon bushings.

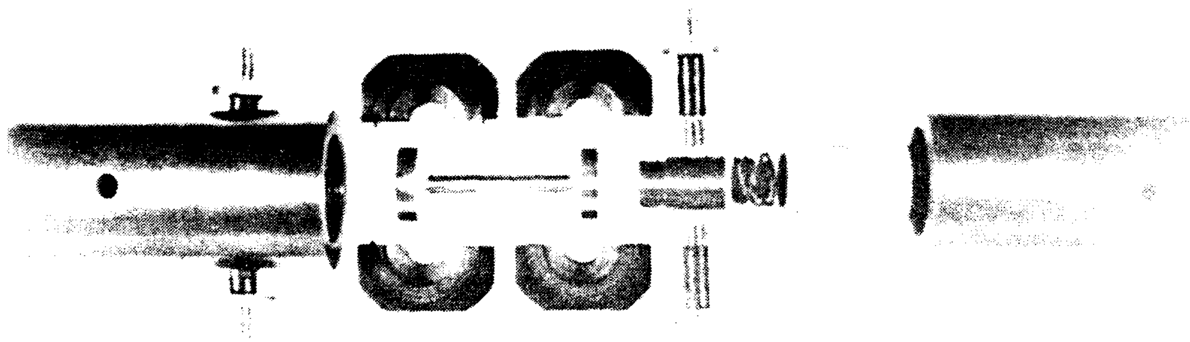

Figure 14. Complete grip assembly.

Specimens are shielded from the atmosphere to prevent the oxidation by an environment chamber which has openings for strain and temperature monitors. The chamber is overpressurized with inert gas. One of the difficult problems encountered in the high temperature mechanical testing is the measurement of strains, particularly at dynamic conditions (high strain rates such as those tests performed in this study). The maximum

5. SMYTHE, W. R. *Static and Dynamic Electricity, Third Edition.* McGraw-Hill, New York, 1968.

temperature which can be sustained by the wire strain gages is approximately 270°C. The high temperature gage made by plasma spray can be used up to 550°C to 830°C, but the cost is too prohibitive to be used in the destructive testing. Clip gages and extensometers constitute alternate measuring techniques, but they are mechanically fragile and must be removed prior to specimen failure. Furthermore, the maximum response time of ordinary extensometers is about 10 Hz, which is much too slow for the high strain rate test. Laser has been utilized in the optical tracking method[6] which requires attaching two flags to the specimen as targets to be tracked. The disadvantage is that at large plastic deformations, the targets could be out of range of the viewport.

Since there were no extensometers available that could meet the requirements of being able to withstand high temperatures and fast response time to measure strains at strain rates up to 50 sec^{-1}, a special optical extensometer was designed and built. The principle of operation of this device is based on the detection of changes in light intensity. The light intensity is varied by the relative displacement of two contiguous, evenly spaced diffraction gratings on two flat, quartz lens which are in intimate contact with each other. The gratings were composed of vacuum-deposited chrome which was later chemically etched to produce a grid system of alternating lines and spaces of equal widths. The grating used in this study was 1968.5 lines per cm which gives a resolution of 0.00051 cm/fringe. The width of spacings has a deviation of less than 1%. Lenses are mounted in metal sliders with the two grid surfaces contacting each other. The metal sliders are, in turn, spring loaded to the specimen with a wedge to ensure the intimate contact during the test. The relative displacement of the two gratings produces a diffraction pattern. The diffraction pattern was monitored by a reflective optical switch which consists of an infrared light-emitting diode and an optically matched phototransistor in the same package. The reflective optical switch is excited by a 5-volt direct current battery to eliminate any alternating current fluctuations. Reflected light intensity is modulated by lens displacement, and the variation is sensed by a photoresistor and converted into an electrical impulse which, in turn, is amplified and recorded. The optical switch has a rise time of 6 μ sec which is equivalent to 66 kHz. Based on the frequency response of optical switch, the allowable maximum strain rate within the capability of the switch can be determined. Since the velocity or displacement rate, d, is given by

$$d = (\text{frequency}) \times (\text{wave length}) \tag{5}$$

where wave length is the grid line spacing, the strain rate ε is

$$\varepsilon = d/(\text{gage length}) = \frac{(\text{frequency}) \times (\text{wave length})}{\text{gage length}} . \tag{6}$$

Therefore, for a grid spacing of 0.00051 cm (5000 lines/inch) and the gage length of 2.86 cm, the strain rate is

$$= \frac{66{,}000 \times 0.00051}{2.86} = 11.8 \text{ sec}^{-1} \tag{7}$$

which is larger than the strain rate of approximately 5 sec^{-1} used in this study.

6. MARION, R. H. *A New Method of High-Temperature Strain Measurement.* Experimental Mechanics, v. 18, no. 4, April 1978, p. 134-140.

The lenses are mounted in sliders with ceramic knife edges (Figure 15). To maintain proper alignment and contact, a second set of sliders is mounted opposite the first set. Spring-loaded tie bolts connect opposite sliders and provide clamping action. Ceramic knife edges secure the sliders to the specimen, and also provide thermal and electric isolation for the gage. The gage length is represented by the initial distance between knife edges. At fracture, the sliders separate and each half remains attached to its portion of the specimen. Reassembly simply requires slipping the two halves together.

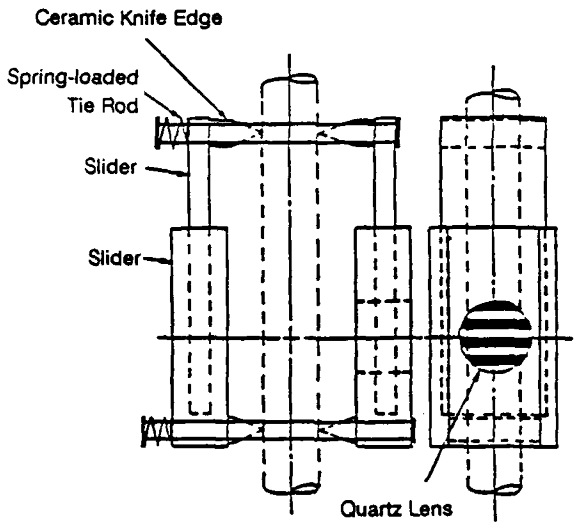

Figure 15. Lens assembly of optical extensometer.

In order to measure the effect of heating rate on mechanical properties of SiC/Al, the loading rate must also be high. In other words, the test time must be very short in comparison to the total heating time to the prescribed temperature. To perform such a test, a test machine with a capability of pneumatic operation is used in this study. Nitrogen is used as a medium for driving the piston. Two fast acting valves are used to evacuate either the top or bottom of the piston, creating a pressure differential which caused the piston to move. Control over the piston's speed is accomplished by varying orifice sizes in the fast acting valves, the pressure of nitrogen, and the length of travel by the piston. In this manner, a nominal strain rate would be achieved which, of course, also depends on the ductility of the material.

Temperature is measured by either thermocouple or by a noncontact optical pyrometer. The signals from load cell, optical extensometer, and thermocouple/pyrometer are recorded by a transient recorder with a sample rate of 2 MHz. The data are stored in a memory first, then played back and analyzed after the test.

During heating, the specimen will increase in length depending on its coefficient of thermal expansion. This occurrence will cause unloading such that a specimen loses contact with the grips. Under this circumstance, free run will occur in the early test time and will be followed by impact loading when specimen and grips come in contact. To eliminate impact

loading, the specimen is preloaded prior to heating. The amount of preload required varies with test temperature, but must be kept below the proportional limit.

The autotransformer setting required to provide the voltage for the prescribed heating rate is calibrated by attaching a thermocouple to the specimen and recording its time history. For heating rate below 1000°C/sec, the response of the thermocouple is fast enough to satisfy the requirement.

Test Results and Discussion

The objectives of this part of the study are twofold. One is to characterize the material at high temperature, high heating rate, and strain rate, while the other is to study the effect of whisker reinforcement on the mechanical properties at such conditions.

Tensile tests of SiC/2014-T4 Al and matrix alloy 2014-T4 aluminum were performed at high temperature, high heating rate, and high strain rates. The test conditions for SiC/2014-T4 Al and 2014-T4 aluminum are listed in Table 3. Test results are shown in Figures 16 through 19.

Table 3. TEST CONDITIONS FOR SiC/2014-T4 AND 2014-T4 ALUMINUM

Material	Temperature (°C)	Heating Rate (°C/sec)	Holding Time (sec)	Strain Rate (sec^{-1})
SiC/2014-T4	RT	N/A	N/A	≅5
	540	250	None	≅5
	540	28	30	≅5
2014-T4	RT	N/A	N/A	≅5
	260	110	None	≅5
	288	14	30	≅5
	540	250	None	≅5

Heating rate and holding time effects were demonstrated in Figures 17 and 19. The results in Figure 17 show that the modulus of 2014-T4 Al has been reduced from 71.7 GPa to 49.0 GPa at 260°C with 110°C/sec heating rate, but it is further reduced to 42.7 GPa when the heating rate is 14°C/sec and the temperature was held for 30 seconds. Meanwhile, the average ductility was increased from 30 percent to 50 percent, and further to 80 percent, if the temperature was held for 30 seconds.

One should notice that the high temperature, high heating rate, and short holding time do reduce the modulus. However, the modulus is much higher than that listed in the handbook because the values in the handbook are obtained after the specimen has been soaked in the temperature for a long time.[7]

Results from tests of SiC/2014 Al at the temperature of 540°C and two different heating rates are shown in Figure 18. For the heating rate of 250°C/sec and no holding time, the modulus is 80 GPa, and the ductility is approximately 2.5 percent. When the heating rate is 28°C/sec and the temperature is held for 30 seconds, the modulus is reduced to 53.8 GPa, and the ductility is reduced somewhat rather than increased. This point will be discussed later.

7. Aerospace Structural Metals Handbook. v. 3, 1979, p. 25.

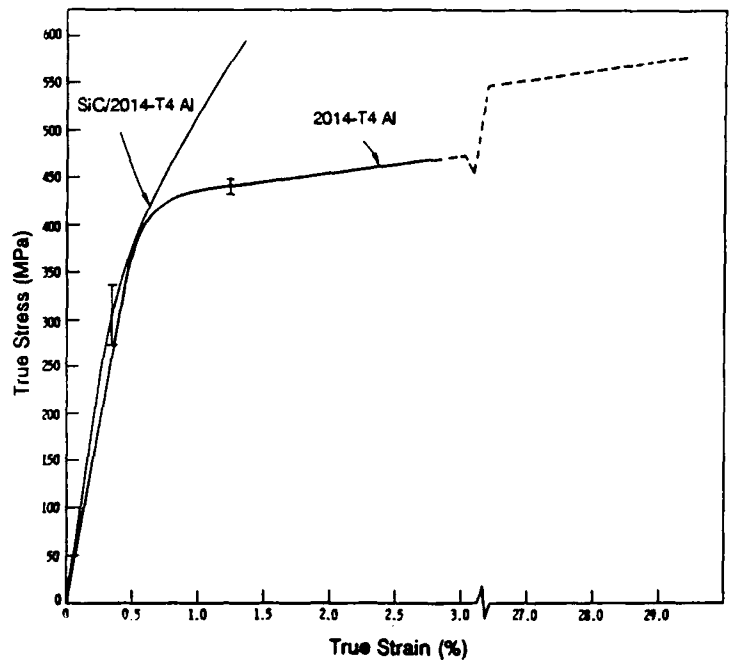

Figure 16. Tension test of 2014-T4 aluminum and SiC/2014-T4 aluminum at room temperature and a strain rate of 10^{-4} sec^{-1}.

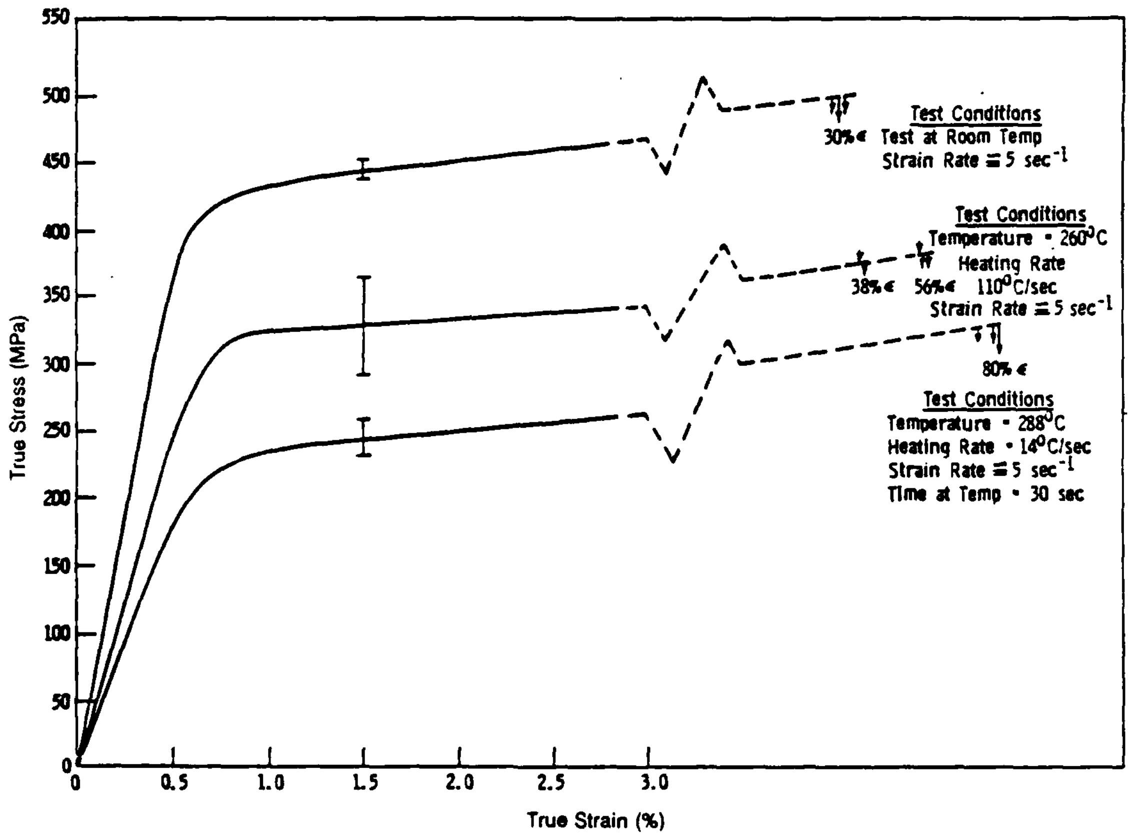

Figure 17. Tensile stress-strain curves of 2014-T4 aluminum tested at various conditions.

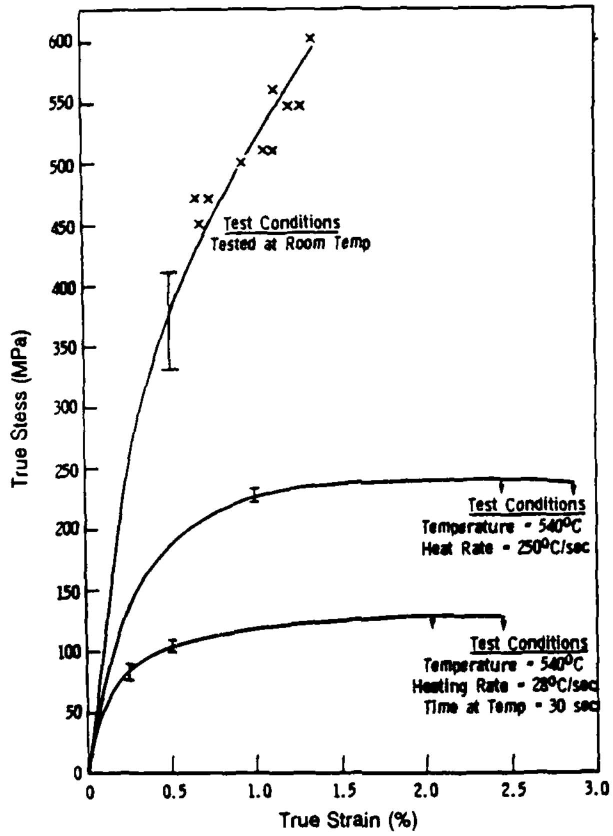

Figure 18. Tensile stress-strain curves of SiC/2014-T4 aluminum tested at various conditions.

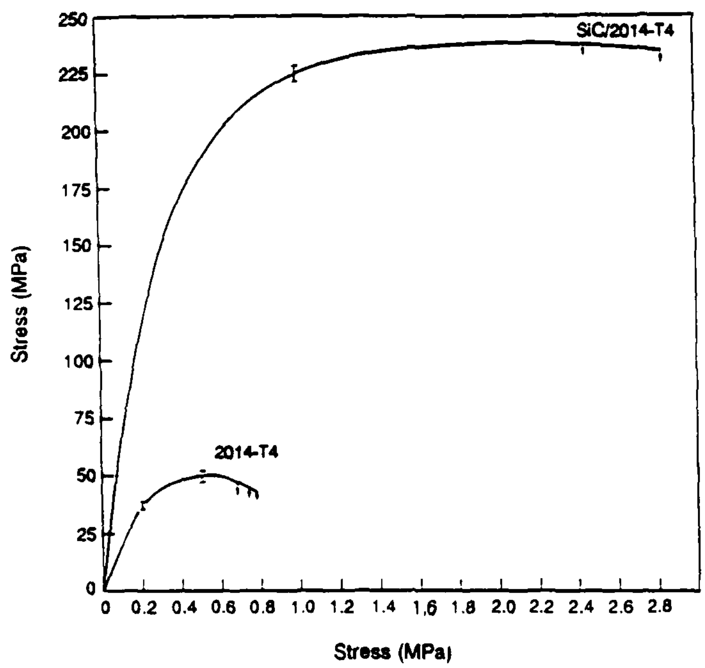

Figure 19. Tensile test of SiC/2014-T4, 2014-T4 aluminum at strain rate of 5 sec^{-1} and temperature of 540°C heated at 250°C/sec.

Finally, Figure 19 shows the comparison of stress-strain curves of SiC/Al and 2014-T4 at a temperature of 540°C heated up at 250°C/sec. The modulus of 2014-T4 Al is about 22 GPa, but with whisker reinforcement, the modulus is 80 GPa, which is almost the same as that of the matrix alloy at ambient temperature. It is interesting to notice that at 540°C, the ductility of 2014-T4 is less than 1 percent, due to the oxidation and decohesion at the grain boundaries.

To answer some of the questions raised by observing the mechanical (tensile) behavior, the fracture surfaces of tested specimen were examined under scanning electronic microscope (SEM). Figure 20 shows the fracture surface of an SiC/Al specimen test at ambient temperature. The silicon carbide whiskers are visible and many dimples of shear lips indicate the local ductile fracture in the matrix alloy.

Figure 20. Typical fracture surface of SiC/Al tested at room temperature, Mag. 5000x.

The fracture surfaces of a SiC/Al specimen tested at 540°C are also examined. The specimen clearly shows a primary crack initiation starting from the center of the specimen. At 5000x magnification, Figure 21 shows fiber pullout at the center of the specimen, an indication of interfacial debonding. The short shear lips in the matrix alloy with rounded edges are indications of localized melting and oxidation which is over all of the fracture surface. The periodic striation at the shear lips indicates that fiber pullouts are random, localized

microoccurrences. At the edge of the specimen in Figure 22, matrix cleavage occurs where there are practically no whiskers and decohesion at grain boundaries, which is caused by heating and oxidation at the grain boundaries. It is known that the 2014 aluminum is an Al-Cu alloy with the eutectic temperature equal to 540°C, at which the specimens were tested in this study.

Summary

Room Temperature Results

The metal-matrix composite material, consisting of randomly dispersed and oriented 25-volume-percent silicon carbide whiskers in a 2014-T4 Al alloy matrix, was tested at various conditions. It was found that the elastic modulus was increased by 60 percent to 120.7 GPa in comparison with that of the matrix material. However, the ductility was significantly reduced to less than 2 percent of strain.

Torsion test of a circular rod gave the relationship between torque and twist angle from which the shear modulus was calculated to be approximately 44.8 GPa. The maximum twist angle per unit length around 1.57 degree/mm also indicated the brittle nature of the material.

The Bauschinger effect was investigated by precompressing the specimens to two strain levels before reversing the load to tension and fracturing the specimens. Results indicated that the material possesses a fixed total available tensile strain of approximately 1.5 percent which was not affected by precompression levels used in this study.

The mode I fracture toughness value, K_{Ic}, was measured with an average value of 13.5 MPa $\sqrt{m}$ which was consistent with low ductility exhibited in tension tests.

High Temperature - High Heating Rate Results

Test results indicate that at the same strain rate, 2014-T4 aluminum exhibits decreasing modulus with increasing temperature, decreasing heating rate, and increasing holding time, while ductility increased under the same condition until the eutectic temperature 540°C was reached, at which point, the grain boundary decohesion and oxidation took place and ductility was drastically reduced.

For SiC/2014 Al, the whisker reinforcement has increased the modulus at ambient temperature to 120.7 GPa, which is 60 percent higher than that of the matrix alloy, but drastically reduced the ductility to 1.5 percent. At high temperature, the modulus decreases but retains a large portion of it even at the eutectic temperature of the matrix alloy. For instance, the modulus at 540°C heated up at 250°C/sec is 80 GPa which is slightly higher than the modulus of the matrix alloy at room temperature. Based on these results, it seems that it is advantageous to use SiC/Al instead of aluminum in a situation where the temperature is too high for the aluminum alloy to sustain.

Figure 21. Fractuer surface at the center of SiC/Al specimen tested at temperature of 540°C (1000°F), Mag. 5000x.

Figure 22. Fracture surface at the edge of SiC/Al specimen tested at temperature of 540°C (1000°F), Mag. 5000x.

PRESSURE DEPENDENCE OF THE ELASTIC CONSTANTS

Introduction

This section deals with the variation in the elastic constants of SiC/2014-T4 Al composite at elevated pressures to 1.5 GN/m^2 (GPa). Obtaining the values of the elastic constants of this composite at elevated pressure allows researchers (1) to determine the equation of state, and (2) to verify theoretical models which estimate the elastic constants of this composite, not only at ambient pressure but also at elevated pressures, from knowledge of the pressure dependence of the elastic constants of its constituents, SiC whiskers, and 2014 aluminum alloy. As high pressure elastic constants data are not available for SiC, use of shock wave data for SiC was made to estimate the values of its elastic constants at high pressures. These estimates of the elastic constants of SiC in conjunction with the high pressure elastic constants data of 2014-T6 aluminum were used to compute elastic constants of the composite at elevated pressure. To our best knowledge, this is the first time such calculations have been done for any composite. Comparisons are made between a model due to Hashin and Shtrikman[8] and a model recently developed by Maewal and Dandekar,[9] which is based on a generalization of the method developed by Mori and Tanaka,[10] Taya and Chou,[11] Weng,[12] and Tandon and Weng[13] for composites in which inclusions are either spherical or oriented along some direction.

In the following paragraphs, specimen configurations and the ultrasonic technique used to determine the elastic constants of the composite, results of the ultrasonic experiments, a brief outline of technique to estimate pressure derivatives of the elastic constants of SiC from the shock wave data, calculations of the elastic constants of the composite on the basis of the elastic constants of its two constituents SiC and 2014-T4 aluminum, and conclusions based on this research are described.

Specimens and Ultrasonic Technique

Right circular solid cylindrical specimens of SiC/Al composite used for the measurements of the elastic wave velocities had their faces either normal to the axis of the thick-walled cylinder (z axis) or normal to the radial direction (r) of the thick-walled cylinders (Figure 23). The specimens of SiC/Al with face normal in z and r directions are, respectively, identified as SiC/Al (z) and SiC/Al (r) in this report.

Elastic wave velocities in SiC/Al (z) and SiC/Al (r) were determined at room temperature; i.e., 295 ± 2°C to detect presence of elastic anisotropicity in the material. Elastic wave velocities at elevated pressures, and at room temperature, were measured only in SiC/Al (z) because the room temperature measurements of the elastic wave velocities in SiC/Al (z) and SiC/Al (r) failed to indicate elastic anisotropy in SiC/Al (see the section on experimental results).

8. HASHIN, Z., and SHTRIKMAN, S. *A Variational Approach to the Theory of the Elastic Behaviour of Multiphase Materials.* J. Mechanics and Physics of Solids, v. 11, 1963, p. 127-140.
9. MAEWAL, A., and DANDEKAR, D. P. *Effective Thermoelastic Properties of Short-Fiber Composites.* Acta. Mech., v. 66, 1987, p. 191-204.
10. MORI, T., and TANAKA, K. *Average Stress in Matrix and Average Elastic Energy of Materials with Misfitting Inclusions.* Acta. Metallurgica, v. 21, 1973, p. 571-574.
11. TAYA, M., and CHOU, T. W. *On Two Kinds of Ellipsoidal Inhomogeneities in an Infinite Elastic Body: An Application to a Hybrid Composite.* International Journal of Solids and Structures, v. 17, 1981, p. 553-565.
12. WENG, G. J. *Some Elastic Properties of Reinforced Solids, with Special Reference to Isotropic Ones Containing Spherical Inclusions.* International Journal of Engineering Science, v. 22, 1984, p. 845-856.
13. TANDON, G. P., and WENG, G. J. *The Effect of Aspect Ratio of Inclusions on the Elastic Properties of Unidirectionally Aligned Composites.* Polymer Composites, v. 5, 1984, p. 327-333.

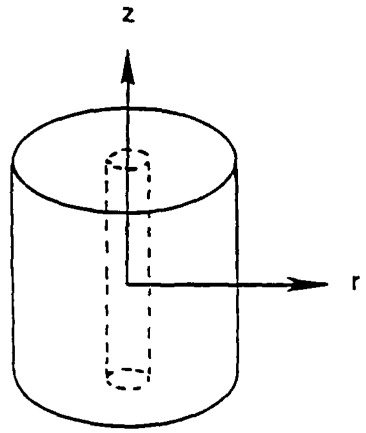

Figure 23. A schematic of the thick-walled cylinders of SiC/Al with its z and r orientation direction.

The specimens of SiC/Al used for the elastic wave velocity measurements at the ambient condition were right circular cylinders with a diameter of 25.5 ± 0.5 mm and a thickness of 38.06 ± 0.01 mm. The specimen of SiC/Al (z) used for the measurements of elastic wave velocities at elevated pressures was a right circular cylinder with a diameter of 12.5 ± 0.1 mm and a thickness of 11.821 ± 000.2 mm. It is identified as the small specimen, when necessary, as in Table 1.

Elastic wave velocities in SiC/Al were measured by the pulse-echo overlap technique developed by Papadakis.[14] In the Papadakis method, the echoes are overlapped on the cathode tube screen by triggering the oscilloscope at a frequency which corresponds to the inverse of transit time between echoes. The correct cycle and, hence, the correct time for the echo in the pulse-echo overlap technique is difficult to discern. The following method was suggested, based on the properties of a composite resonating system. The resonant frequency of the transducer is found, a cycle overlap is chosen for the two echoes, and the transit time is found. The frequency exiting the transducer is then reduced to nine-tenths of the resonant frequency, and the transit time, thus obtained, for the same cycle overlap is subtracted from the transit time obtained when the resonant frequency was used. This procedure is followed when the cycle for cycle overlap between the two echoes is switched by one cycle at a time. The differences in times, thus obtained, should change by a constant amount as one progresses from cycle to successive cycle comparisons.

The correct cycle overlap can then be found by noting the spacing of the difference in transit times obtained above, as the cycles of overlap are changed one at a time. The method of choosing the correct cycle for overlap is discussed further in Ref. 14. We found, however, that some uncertainty is removed from the selection by repeating the above procedure with a transducer of a different frequency. In that case, all the intervals mentioned above should change, but the correct cycle overlap retains the same value. The velocities at the resonant frequency of each transducer should equal each other at the correct overlap.

14. PAPADAKIS, E. P. *Ultrasonic Phase Velocity by the Pulse-Echo-Overlap Method Incorporating Diffraction Phase Corrections.* Journal of the Acoustical Society of America, v. 42, 1967, p. 1045-1051.

This method assumes that there is no dispersion of sound waves in the material. This technique was used only on the small specimen subjected to high pressure.

The longitudinal and shear wave velocity data on large specimens were obtained at 10 MHz and 5 MHz, respectively. The longitudinal and shear wave velocity measurements in the small specimen were made at two different frequencies; i.e., 10 and 15, and 5 MHz and 10 MHz, respectively. During the measurements of transit times between echoes at elevated pressures, only changes in times were measured. Nine sets of measurements were performed as a function of pressure; three of these were for longitudinal velocity mode, and the remaining six with random polarization were for shear velocity mode. The absolute velocity values are estimated to have an accuracy of 2×10^{-3}.

Pressure was generated in a Birch-Bridgman high pressure cell manufactured by Harwood Engineering Co., Inc., Walpole, MA. The pressure medium was a 50/50 mixture of Pentane/Isopentane. The pressure was determined by a Manganin coil calibrated via a dead weight tester.

Results of Ultrasonic Experiments

Table 1 summarizes the results of measurements performed on the specimens of SiC/Al at the ambient condition.

The densities of SiC/Al were measured by the immersion technique. Measured densities of nine specimens of each of the two orientations; i.e., SiC/Al (z) and SiC/Al (r), were determined to be 2.908 ± 0.028 and 2.904 ± 0.0006 Mg/m^3, respectively. The expected density of the present composite composed of 25-volume-percent SiC with a density of 3.21 Mg/m^3 and 75-volume-percent 2014-T4 aluminum with a density of 2.81 Mg/m^3 was calculated to be 2.910 Mg/m^3. Thus, the measured densities of SiC/Al used in the present investigation are not significantly different from the theoretical density of the composite and, hence, can be considered to be pore free. The average density of the above mentioned 18 density measurements is 2.906 ± 0.02 Mg/m^3 for SiC/Al. This value of density is used in all the subsequent calculations.

Elastic Constants at the Ambient Condition

Velocities of three elastic waves were determined in each of the nine large specimens of SiC/Al (z) and SiC/Al (r). The two shear wave velocity modes were measured to yield a maximum difference in their measured values. These shear wave velocities are identified as Shear (1) and Shear (2) in Table 1. The values of elastic wave velocities given in Table 1 do not appear to be significantly different in SiC/Al (z) and SiC/Al (r) directions. Hence, it is concluded that the composite SiC/Al used in the present work is elastically isotropic. The representative values of longitudinal and shear wave velocities for this composite, calculated as the arithmetic average of the respective velocity measurements, are 7.307 ± 0.05 and 3.884 ± 0.027 km/sec, respectively. It should be noted that even though the precisions of the density and elastic wave velocity measurements are no worse than 0.2%, the actual errors associated with these parameters are larger and around 0.7%, possibly due to materials variability of the 19 specimens of SiC/Al used in these measurements. Thus, one may regard the variability in the values of the above mentioned three parameters of SiC/Al as inherent in the method of fabrication of this composite.

Table 4 gives the values of densities and elastic properties of SiC/2014-T4 Al and 2014-T4 measured in the present work. The values of these parameters for SiC and 2014-T6 are from Ref. 15 and 16, respectively. The values of density and elastic constants of the last three materials are also subsequently used to calculate the elastic constants of SiC/2014-T4 Al based on theoretical models for composites due to Hashin and Shtrikman[8] and Maewal and Dandekar.[9]

Table 4. DENSITY AND ADIABATIC ELASTIC PROPERTIES OF SiC/2014-T4 Al, SiC, 2014-T4 Al, AND 2014-T6 Al

Properties	Units	SiC/2014-T4 Al*	SiC†	2014-T4 Al*	2014-T6 Al‡
Density	Mg/m^3	2.906	3.21	2.81	2.81
Elastic Wave Velocity	km/sec				
Longitudinal V(1)		7.307	12.37	6.378	6.353
Shear V(s)		3.884	7.81	3.145	3.199
Bulk V(b)		5.769	8.47	5.243	5.169
Elastic Modulus	GPa				
Young's (E)		114 ± 2	458.0	74.5	76.4
Shear (μ)		43.8 ± 0.7	196.0	27.8	28.7
Bulk (K)		96.7 ± 1.3	230.2	77.2	75.1
Poisson's Ratio (ν)		0.303 ± 0.006	0.168	0.341	0.330
Pressure Derivative					
Bulk Modulus		5.42	2.8**		4.23
Shear Modulus		2.48	2.9**		2.25

*Present work
†Ref. 15
‡Ref. 16
**Estimated from shock data, see text for details

Elastic Constants at Elevated Pressures

The changes in the elastic wave velocities in SiC/Al were obtained from the measured changes in frequencies of longitudinal and shear wave modes as a result of changing the pressure. The results of three sets of frequency measurements for longitudinal wave velocities and six sets of similar measurements for shear wave velocity in SiC/Al are shown in Figures 24 and 25, respectively. These figures show that measured frequencies for both longitudinal and shear wave velocities in SiC/Al vary almost linearly with pressure. The least squares fit to these data yield

$$F(1,P)/F(1,0) = 1.00010 + (2.61363 \times 10^{-2})P \tag{8}$$

and

$$F(s,P)/F(s,0) = 0.998949 + (2.70908 \times 10^{-2})P \tag{9}$$

for longitudinal and shear wave velocities, respectively, to 1.5 GPa.

15. SCHREIBER, E., and SOGA, N. *Elastic Constants of Silicon Carbide.* Journal of the American Ceramic Society, v. 49, 1966, p. 342.
16. BABCOCK, S. G., LANGAN, J. J., NORVEY, D. B., MICHAELS, T. E., SCHIERLOH, F. L., and GREEN, S. G. *Characterization of Three Aluminum Alloys.* U.S. Army Materials Technology Laboratory, AMMRC CR 71-3, January 1971.

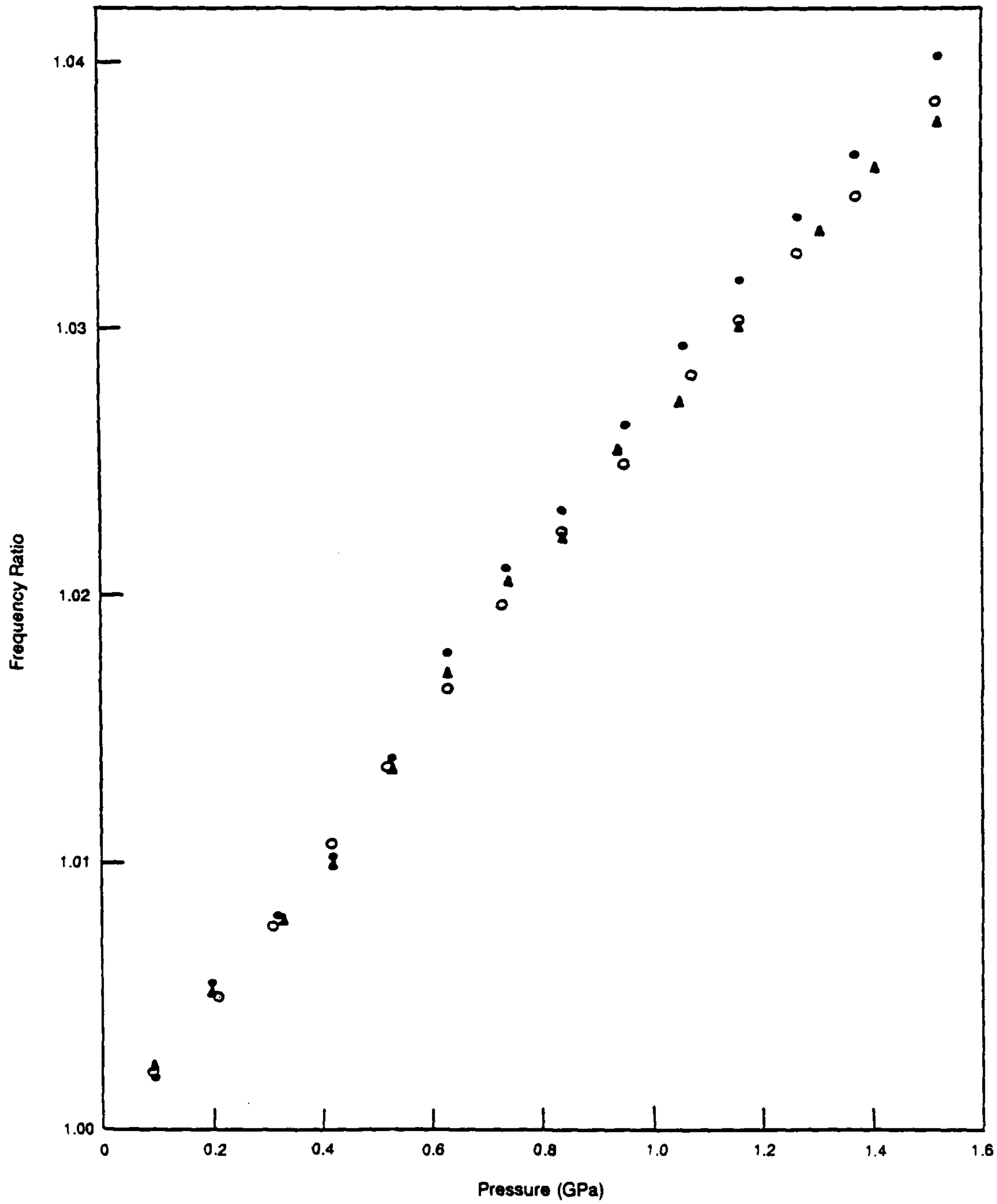

Figure 24. Frequency ratio for longitudinal elastic wave velocity versus pressure in SiC/Al in three different experiments.

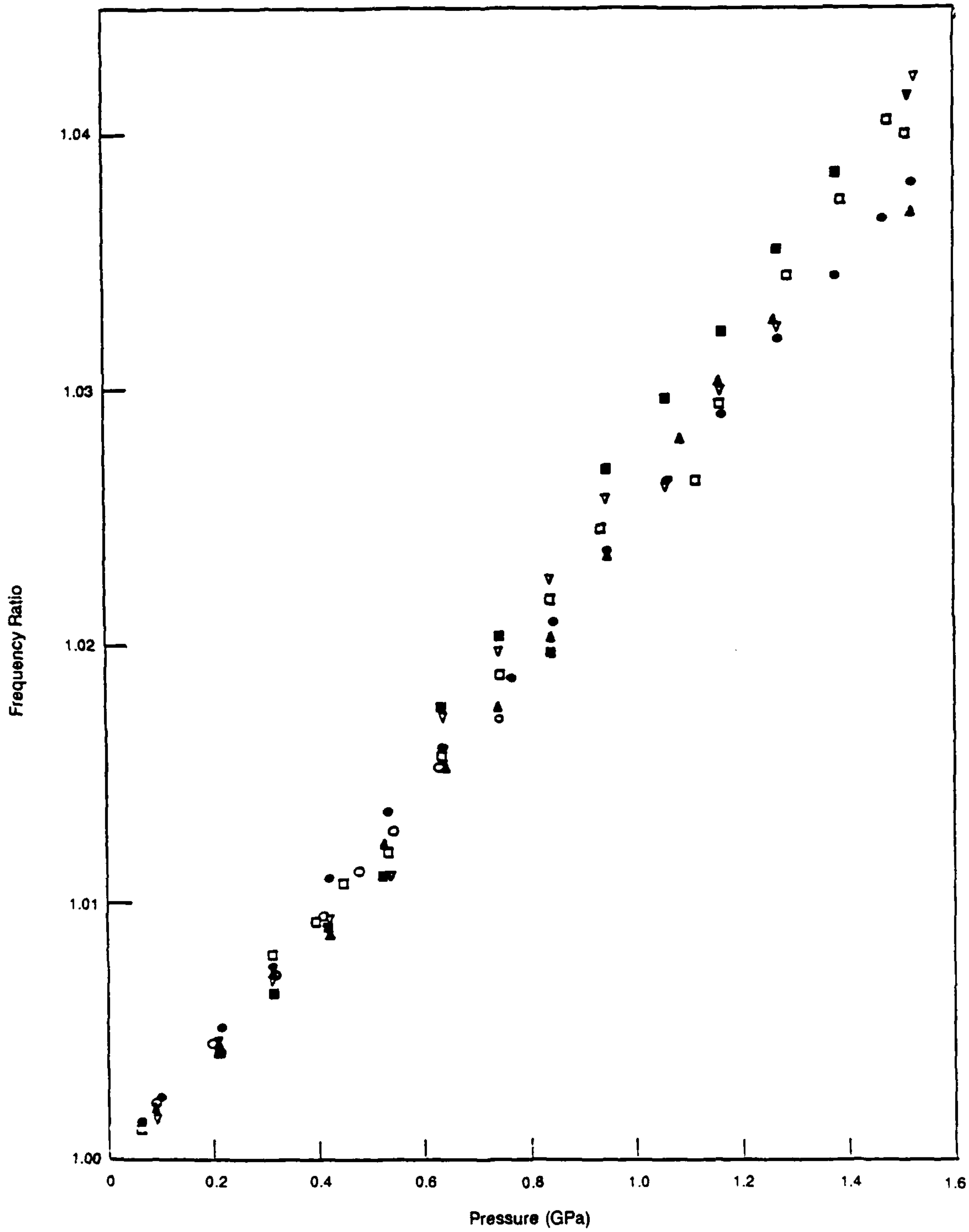

Figure 25. Frequency ratio of shear elastic wave velocity versus pressure in SiC/Al in six different experiments.

In the above equations, P is pressure in GPa. In Equation 8, F(1,P) and F(1,0) are the frequencies (reciprocal of transit time for elastic wave) for longitudinal elastic wave at pressure P and one atmospheric pressure, respectively. Similarly, in Equation 9, F(s,P) and F(s,0) are the frequencies for shear elastic wave at pressure P and one atmospheric pressure, respectively. The correlation coefficient for these respective least squares fits are 0.9987 and 0.995.

It should be noted that under ideal circumstances, the first coefficients in Equations 8 and 9 would be identical and equal unity. However, in the subsequent calculations, we have used Equations 8 and 9 so as not to artificially remove the inherent error incurred in representing the frequency variations with pressure by a straight line. The changes in the elastic wave velocities and elastic constants with pressure were calculated by applying the self-consistent iterative method to obtain the numerical values of these constants without a prior knowledge of the compressibility of the material developed by Dandekar, the details of which can be found in Ref. 17. These computations require values of volume thermal expansion coefficient (β) and specific heat at constant pressure (Cp). Since the value of β is not yet measured for SiC/2014-T4 Al, the measured value of the volume thermal expansion coefficient for a composite consisting of 25-volume-percent SiC whiskers in 2024-T6 aluminum matrix is used instead. The value of β is $5.076 \times 10^{-5} \times {}^{o}K^{-1}$.[18] Similarly, the value of the specific heat is computed by using the thermal model given in Ref. 19 and the measured values of specific heat, thermal expansions, and bulk moduli of SiC and 2014-T6 aluminum. The calculated value of Cp for SiC/2014-T4 is 919.6 $J/kg^{-1}\ {}^{o}K^{-1}$. These values of β and Cp were used because their values for SiC/2014-T4 aluminum remains to be determined. However, it can be shown that even an error of 10% in the values of either of these two parameters will change the calculated values of elastic constants by only 0.4%. Isothermal pressure derivatives of adiabatic bulk and shear moduli of SiC/2014-T4 determined from the sound wave velocity measurements are displayed in Table 4.

These pressure derivatives can be used with confidence to 1.5 GPa and probably may be used above this pressure to obtain pressure-volume curve to a much higher pressure.

The adiabatic compression curve of SiC/2014-T4 Al when expressed in the form of Bridgman's equation; i.e.,

$$-\Delta V/V_0 = aP + bP^2 \qquad (10)$$

where a is adiabatic compressibility; i.e., K^{-1} and

$$b = -0.5\ \{1 + (\delta K\ /\ \delta P)_T\}\ /\ K^2(P) \quad \text{as } P \longrightarrow 0 \qquad (11)$$

and V/V_0 is the change in volume with respect to the volume V_0 of the material at the ambient pressure, is given by

$$-\Delta V/V_0 = (1.0341 \times 10^{-2})\,P - (3.4323 \times 10^{-4})P^2\ . \qquad (12)$$

17. DANDEKAR, D. P. *Iterative Procedure to Estimate the Values of Elastic Constants of a Cubic Solid at High Pressures from the Sound Wave Velocity Measurements.* Journal of Applied Physics, v. 41, 1970, p. 667-672.
18. GUBBAY, J. D. *Micromechanical Properties of Al/SiC Metal Matrix Composite.* The Charles Stark Draper Laboratory Final Reports CSDL-R-1578, The Charles Stark Draper Laboratory, Inc., Cambridge, MA, June 1982.
19. CHRISTENSEN, R. M. *Mechanics of Composite Materials.* John Wiley and Sons, New York, 1979, p. 311-339.

Discussion

It is of interest to note that the pressure derivatives of the elastic moduli obtained for SiC/2014-T4 Al exceed the respective pressure derivatives for 2014-T6 Al. Since tempering of 2014 Al to T4 and T6 conditions do not change their elastic constants significantly, it is reasonable to assume that the pressure derivatives of the bulk and shear moduli of 2014-T4 Al could not be significantly different from those experimentally determined for 2014-T6 Al in Ref. 16. Unfortunately, no high pressure elastic constant measurements of SiC are yet available for such a direct comparison. However, one can estimate the pressure derivatives of the bulk and shear moduli of SiC by using the existing shock wave data given in Ref. 20 and 21. McQueen, et al.,[20] showed that the shock wave velocity, U_s, in SiC was linearly dependent on the particle velocity, U_p and this dependency can be written as

$$U_s = 8.00 + 0.95\ U_p \tag{13}$$

where U_s and U_p are in km/sec. This relationship was determined by conducting shock wave experiments where the maximum pressure reached in SiC was 110 GPa. Whenever such a linear relationship is found to exist for a material, it implies that the pressure derivative of the bulk modulus (K') for the material as the pressure goes to zero is given by

$$K' = 4s - 1 \tag{14}$$

where s is the rate of change of U_s with respect to U_p; i.e., for SiC, the value of s is 0.95 as in Equation 13. Therefore, the value of the pressure derivative of the bulk modulus is 2.8. It is this value which is listed in Table 4 for SiC.

The shear modulus of SiC at high pressure is calculated from the relation between the modulus μ, and the Hugoniot Elastic Limit (HEL) σ_H, relative volume change at HEL η_H, and Hugoniot pressure P_H, at η_H.[22] Hugoniot pressure P_H, at low pressures, for instance below 10 GPa, is very close to hydrostatic pressure. Therefore, the shear modulus μ, at pressure P_H is given by

$$\mu = 0.75\ (\sigma_H - P_H)\ /\ \eta_H \tag{15}$$

where $\eta_H = 1 - V_H / V_0$.

The average value of η_H for SiC on the basis of eight shock wave experiments where HEL was observed in Ref. 21 is found to be 1.92×10^{-2}. The average initial density of SiC used by Gust, et al.,[21] was 3.08 Mg/m^3. The observed HEL for this low density SiC was 8.0 GPa.

The value of σ_H for fully dense SiC, assuming that η_H does not depend on porosity, can be estimated from the equation

$$\sigma_H = \rho_0\ V^2(1,0)\ \eta_H \tag{16}$$

20. McQUEEN, R. J., MARSH, S. P., TAYLOR, J. W., FRITZ, J. N., and CARTER, W. J. in *High Velocity Impact Phenomena.* Ray Kinslow, ed., Chapter V I and Appendix E, Academic Press, New York, 1970, p. 293-417 and p. 549.
21. GUST, W. H., HOLT, A. C., and ROYCE, E. B. *Dynamic Yield, Compressional, and Elastic Parameters for Several Lightweight Intermetallic Compounds.* Journal of Applied Physics, v. 44, 1973, p. 550-560.
22. FOWLES, G. R. *Shock Wave Compression of Hardened and Annealed 2024 Aluminum.* Journal of Applied Physics, v. 32, 1961, p. 1475-1487.

where ρ_0 is the initial density and V(1,0) is the longitudinal velocity at one atmospheric pressure.[23] Substituting the values of ρ_0 and V(1,0) for SiC listed in Table 2, we get a value of 9.44 GPa for σ_H of fully dense SiC.

When a similar correction is done for the determination of P_H for fully dense SiC from the data of McQueen, et al.,[20] we obtain a value of 4.115 for P_H at $\eta_H = 1.92 \times 10^{-2}$. Substituting the values of σ_H, P_H, and η_H in Equation 15 gives a value of shear modulus (μ) equal to 207.9 GPa. This can be treated as the value of μ of SiC at pressure P_H; i.e., 4.115 GPa. The value of shear modulus of fully dense SiC at one atmospheric pressure is 196 GPa (Table 4). Hence, the calculated pressure derivative of the shear modulus is 2.9, as listed in Table 4.

Table 4 shows that the pressure derivative of bulk modulus of SiC/Al is larger than the pressure derivatives of this modulus for each of the two constituents. However, the pressure derivative of the shear modulus of SiC/Al is comparable to those of its two constituents. The physical reason for this is not clear at present.

Following the works of Hashin and Shtrikman[8] and estimates of the elastic constants using the procedure of Maewal and Dandekar,[9] we obtain the numbers given in Table 5. Both models predict elastic constants values for SiC/Al composite by using the elastic constants of its constituents SiC and 2014-T4 Al.

Table 5. ELASTIC CONSTANTS (IN UNITS OF GPa) OF SiC/Al AS A FUNCTION OF PRESSURE

	Pressure (GPa)			
	0.0001		1.5	
	Bulk Modulus	Shear Modulus	Bulk Modulus	Shear Modulus
Measured	96.7	43.8	104.8	47.5
Hashin and Shtrikman				
Lower Bound	96.3	41.3	103.3	45.8 (45.6)
Upper Bound	105.7	54.5	112.1 (112.0)	58.3 (57.7)
Maewal and Dandekar	100.0	45.3	106.7 (106.7)	49.5 (49.2)

Comparison shows that the measured values of the elastic constants of SiC/Al do lie within the Hashin and Shtrikman[8] bounds both at the ambient and elevated pressures. The estimates of bulk and shear moduli following the Maewal and Dandekar[9] procedure are within 4% of the above results. Since the errors involved in the estimation of shear modulus of SiC at high pressure from shock wave data of Ref. 20 and 21 could be large, in Table 5 we include the computed values of bulk and shear moduli of SiC/Al at 1.5 GPa with a drastic assumption that shear modulus of SiC does not change with pressure. These calculations are shown within parentheses in Table 3 and reveal that the calculated values of the constants are only negligibly changed due to this drastic assumption.

23. STEINBERG, D. J. *Equations of State for the Ceramics BeO and B C.* UCID-16946, Lawrence Livermore National Laboratory, Livermore, CA, November 1975.

Conclusions

1. The equation of state of SiC/Al, when expressed in the form of Bridgeman's equation, is given by

$$- \Delta V/V_0 = (1.0341 \times 10^{-2})P - (3.4323 \times 10^{-4})P^2$$

where P is in GPa.

2. The model developed by Maewal and Dandekar seems to provide reasonable estimates of the elastic constants of SiC/Al as a function of pressure and is consistent with the Hashin and Shtrikman bounds.

3. The calculated values of the elastic constants of SiC/Al at high pressure are relatively insensitive to the pressure derivative of the shear modulus of SiC.

COMPRESSION AT HIGH PRESSURES

Introduction

This section deals with the measurement of isothermal compression of the composite; i.e., change in volume of the composite with pressures to 4.5 GPa at room temperature. In general, compression of a material can be measured by insitu X-ray diffraction measurements at high pressure,[24] elastic wave velocity measurements at high pressure,[25] or the information provided in the section of this report titled "Pressure Dependence of the Elastic Constants" and measurements of volume of a material at high pressure.[26] The X-ray diffraction technique is inapplicable to determine compression of an amorphous material or a composite material even though its constituent materials are crystalline. The reason for inapplicability of the X-ray diffraction technique to composites lies in the fact that the constituents of a composite maintain their individual identities, unlike constituents of an alloy. Thus, the composites are a physical mixture of its constituents, and X-ray diffraction would merely provide compressions of each of the constituents of a composite but not of the mixture. On the other hand, the techniques of elastic wave velocity measurements and volume measurements to determine compression of a material are applicable to all materials. The elastic wave velocity measurement in an opaque solid is generally restricted to less than 2.0 GPa, mainly due to difficulty in the construction of a reasonable size pressure chamber which will routinely withstand higher than 2.0 GPa. Therefore, in order to determine the compression of a material above 2.0 GPa, one either extrapolates the results of elastic wave velocity measurements in a material at low pressures to higher pressures, or one can perform volumetric measurements on a material to higher pressure. The practical limit on a pressure chamber for this type of measurement is around 6.0 GPa. In this section, the results of compression measurements on SiC/2014-T4 aluminum composite to 4.5 GPa is compared with the results of elastic wave velocity measurements on the same composite to 1.5 GPa at room temperature presented in the previous section.

24. MAUER, F. A., MUNRO, R. G., PIERMARINI, G. J., BLOCK, S., and DANDEKAR, D. P. *Compression Studies of a Nickel-Based Superalloy, MAR-M200, and of Ni_3Al.* J. Appl. Phys., v. 58, no. 3727, 1985.
25. DANDEKAR, D. P., FRANKEL, J., and KORMAN, W. J. *Pressure Dependence of the Elastic Constants of Silicon Carbide/2014 Aluminum Composite.* Testing Technology of Metal Matrix Composites, ASTM STP 964, P. R. DiGiovanni and N. R. Adsit, ed., American Society for Testing and Materials, Philadelphia, PA, 1988, p. 79-89.
26. VAIDYA, S. N., and KENNEDY, G. C. *Compressibility of 18 Metals to 45 kbar.* J. Phys. Chem. Solids, v. 31, no. 2329, 1970.

Specimen and Experimental Detail

Specimens of SiC/Al used for compression measurements were in the shape of right circular solid cylinders. These specimens were 8.992 ± 0.013 mm in diameter and 12.802- ± 0.025-mm long. The faces of these cylinders were either normal to the axis of the thick-walled cylinder (z axis) or normal to the radial direction (r) of the thick-walled cylinder (Figure 23). The specimens of SiC/Al with face normal in z and r direction are, respectively, identified as SiC/Al (z) and SiC/Al (r), as done previously.

Compressibility of SiC/Al as a function of pressure to 4.5 GPa at room temperature was obtained from the measurement of the axial shortening of the cylindrical specimen of SiC/Al in a solid pressure medium piston cylinder apparatus. A schematic of the sample arrangement and pressure vessel piston assembly for compressibility measurement in the piston cylinder apparatus is given in Figure 26.

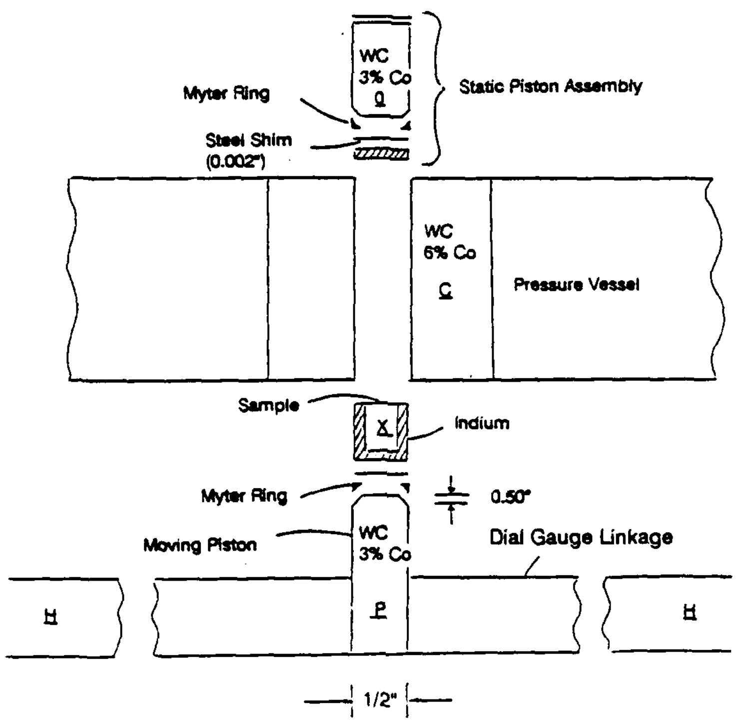

Figure 26. A sketch of sample arrangement and pressure vessel-piston (P) assembly for compressibility measurement in piston cylinder apparatus.

The important details of the apparatus and basic experimental procedure have been described by Viadya and Kennedy.[26] The experimental procedure followed in the present work is the same as given in Ref. 26, but the calculation of volume compression is different from those of Kennedy and coworkers.[26,27] Kennedy and coworkers calculated the volume compression by comparing the change in the length of the sample assembly as a function of pressure with that of a standard sample of known compression in an effectively identical assembly.

27. SINGH, A. K., and KENNEDY, G. C. *Compression of Calcite to 40 kBar.* J. Geophys. Res., v. 79, no. 2615, 1974.

In the present work, calculation of the volume compression of the sample is obtained by calculating the compressibility of the sample assembly as a function of pressure from the axial shortening data, and correcting for the compressibility of other materials in the assembly, and for the dilation of the tungsten-carbide core which contained the pressure cell. Briefly, a cylindrical sample of SiC/Al was completely encased in indium (In) to prevent uniaxial deformation during compression. The diameter and length of the cylinder were 8.992 ± 0.013 mm, and 12.802 ± 0.025 mm, respectively. The dimensions of the In jacket and sample were based on the careful study of Singh and Kennedy[27] who determined the optimal dimensions by trial and error so that there was just enough In to prevent deformation of the sample. The dimensions of a sample recovered after the run was compared with the initial dimensions, and no significant change was observed in any sample, indicating that the pressure environment was very nearly hydrostatic. The In jacket was fabricated by pressing molten In into a die such that it very closely matched the dimensions of the sample cylinder. The thickness of In between a sample and piston was 2.54 mm, whereas the wall thickness of In surrounding the sample was 1.803 mm (Figure 26). The In jacket was surrounded by a thin 0.052-mm Pb foil in order to minimize mechanical failure of WC core by the ingress of In through the fine cracks that sometimes developed in the WC cores during a high pressure run. The axial shortening of the assembly as a function of pressure was measured in two dial gages with a precision of 0.00127 mm. The mean of the two readings represents the true piston intrusion of a given nominal pressure. The maximum difference between the two dial gage readings was 0.00406 mm. The measurements were made in both compression and decompression cycles at 0.5 GPa intervals after an initial cycling of the assembly to 3.5 GPa. As schematically illustrated in Figure 27, the true pressur corresponding to a given piston intrusion (or axial compression) lies somewhere within the hysteresis loop defined by the compression and decompression measurements. Kennedy and coworkers[26,27] took the mean of the compression and decompression data to represent the true pressure corresponding to a given piston intrusion. However, the true pressure need not be symmetric between the nominal pressures in the compression and decompression cycles. Further, owing to the nature of the hysteresis loop, averaging of the pressure in the compression and decompression measurements could distort the slope of the piston displacement (PD) versus pressure (P), as illustrated in Figure 27. Since it is only the slope of the PD versus P curve that we need in our calculations (see below), we used only the "upstroke" values. If there is essentially a constant friction during the compression cycle within the range of our data, then the "upstroke curve" should be parallel to the true PD versus P curve. If, on the other hand, the friction increases as a function of pressure, as it would if it were a constant percentage of the pressure, then the upstroke PD versus P curve would be flatter than the true curve, making the sample appear somewhat less compressible than what it actually is. This problem cannot be resolved at present, but comparison of our compression data for SiC/Al with the results from ultrasonic measurements do not suggest an underestimation of compressibility of SiC/Al by the above method. The "upstroke" PD versus P data were regressed according to

$$PD = A + (B)P + (C)P^2. \tag{17}$$

Regression using a higher order polynomial led to overfitting of the data, in some cases causing wrong curvature of the calculated volume ratio V(P)/V(0) versus pressure relation where V(P) and V(0) are volumes at elevated and ambient pressure, respectively. The second order polynomial fitted all data with an index of correlation (R) of 0.998.

The compression of the WC piston (6% Co binder) was measured in two "dummy experiments" in which the space for the sample assembly was filled with a piston. The

experimental arrangement was otherwise identical to that used for compression measurement of the samples. The PD versus P data were regressed and normalized by multiplying by the ratio of the piston lengths in the "dummy experiment" and in the sample compression experiment. We, thus, obtain the following expression as the contribution to piston displacement due to compression of the pistons (along with four steel shims, Figure 26) in the measurement of axial compression of sample assembly.

$$PD(Piston) = a + bP$$

$$= 0.2865(10^{-2}) + 0.0842(10^{-4})P; \quad (18)$$

$$r = -0.998$$

where the pressure P is in GPa.

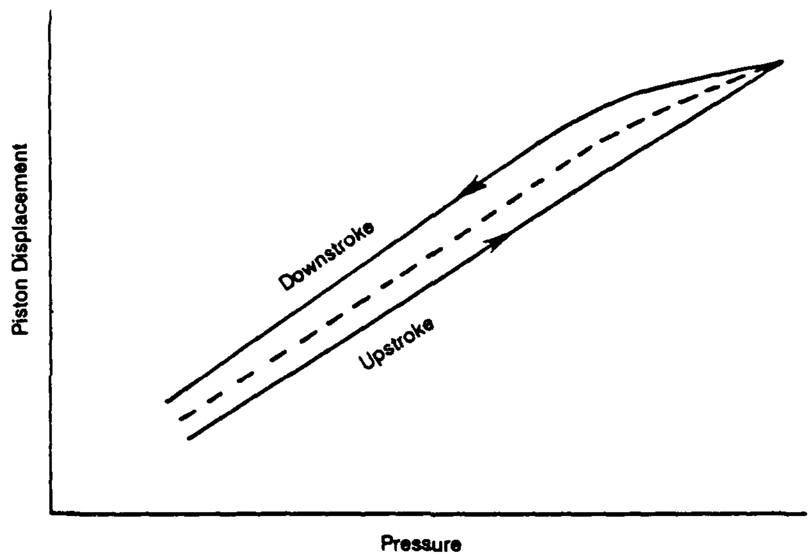

Figure 27. Piston displacement versus pressure during compression (upstroke) and decompression (downstroke).

Calculation of Volume Change

The cross-sectional area of the carbide core of the pressure vessel undergoes dilation as a function of pressure. Vaidya and Kennedy[26] have measured this dilation to 4.5 GPa interval for pressure cores of exactly the same composition (WC 6% Co) as used in the present study. Their data have been fitted to the following expression:

$$\Delta A = 1 + (\alpha)P + (\beta)P^2 \quad (19)$$

where ΔA is the ratio of the cross-sectional area of the core at pressure P and at zero pressure. Constrained statistical regression (r = 0.99997) yields α = 0.8921 (10^{-3}) and β = 0.5575 (10^{-3}) when P is in GPa. According to Equations 17 and 18, the length of the sample assembly at pressure P, l(P), is related to its initial length, l(0), as follows:

$$l(P) = l(0) - B'P - CP^2 \qquad (20)$$

where $B' = (B-b)$. The cross-sectional area of the pressure vessel at pressure P is given by (πr_0^2) (ΔA), where r_0 is the core radius at zero pressure. Thus, the volume of the sample assembly at a pressure P, $V_T(P)$, is related to its length $l(P)$ according to

$$V_T(P) = A_0(\Delta A) \times l(P) \qquad (21)$$

where $A_0 = \pi r_0^2$.

Combining Equations 19, 20, and 21, and rearranging terms, we obtain

$$V_T(P) = V_T(P) - V_T(0) =$$

$$(X_1)P + (X_2)P^2 + (X_3)P^3 + (X_4)P^3 \qquad (22)$$

where $V_T(0)$ is the initial volume of the sample assembly, and

$$X_1 = V_T(0)\,\alpha - A_0B' \qquad (23)$$

$$X_2 = V_T(0) - A_0\alpha B' - CA_0 \qquad (24)$$

$$X_3 = -A_0(B'\beta + \alpha C) \qquad (25)$$

$$X_4 = -A_0\,\beta C. \qquad (26)$$

Vaidya and Kennedy[26] have measured the compressibilities of In and Pb. From these data, and the known volume of In and Pb in each run, we calculated the contributions to $\Delta V_T(P)$ due to the compression of In and Pb.

The residual $\Delta V_S(P)$, which is due to the compression of the sample of interest, is then fitted against pressure according to the constrained form

$$[V_S(P)-V_S(0)] \,/\, V_S(0) = \qquad (27)$$

$$\Delta V_S(P) \,/\, V_S(0) = C_1P + C_2P^2.$$

In the above equation, $V_S(P)$ and $V_S(0)$ are the volumes of the sample; i.e., SiC/Al at pressure P and one atmosphere, respectively. C_1 is identified with isothermal compressibility (K^{-1}) of the material and C_2 is given by

$$C_2 = -0.5\ \{1+(\delta k/\delta P)_T\} \,/\, K^2(P) \text{ as } P \longrightarrow 0 \qquad (28)$$

The results of experiments to determine compressions of SiC/Al (z) and SiC/Al (r) are shown in Figure 28. This figure indicates that compressions of SiC/Al with different orientations are essentially the same. Therefore, the data of compressions on these two types of samples of SiC/Al are combined to yield a relation which represents the isothermal compression of SiC/Al to 4.5 GPa. This relation is

$$V(P)/V(0) = 1 - 1.454 \times 10^{-2}P + 8.9815 \times 10^{-4}P^2. \qquad (29)$$

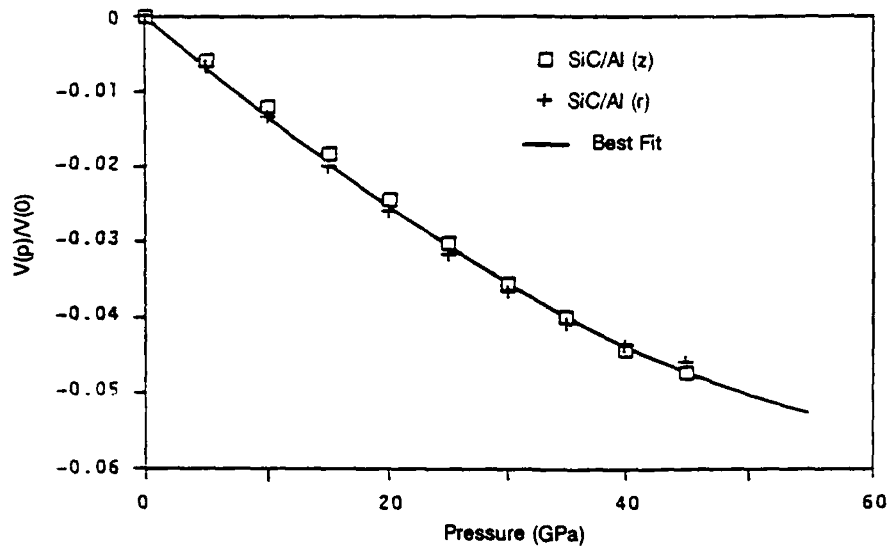

Figure 28. Volume compression of SiC/Al (z) and SiC/Al (r) versus pressure.

Discussion

Isothermal compression of SiC/Al obtained from the measurements of elastic wave velocities as a function of pressure to 1.5 GPa, given in Ref. 25 is represented by

$$V(P)/V(0) = 1 - 1.063 \times 10^{-2}P + 3.5075 \times 10\text{-}4P^2. \tag{30}$$

It is clear from Equations 29 and 30 that the coefficients C_1 and C_2 are not equal. However, if one tabulates the values of V(P)/V(0) obtained from these two equations for various values of pressure (P), it becomes equally evident that the values of volume ratios at a given P are very nearly equal (Table 6). At the highest pressure; i.e., 4.5 GPa, the values of V(P)/V(0) in these two studies differ only by 0.7%.

Table 6. ISOTHERMAL COMPRESSION OF SiC/Al AS OBTAINED IN THE PRESENT WORK AND IN REF. 24 OR THE PRESSURE DEPENDENCE OF THE ELASTIC CONSTANTS SECTION

	V(P) / V(0)	
Pressure (GPa)	Present Work	Pressure Dependence of the Elastics Section
0	1	1
0.5	0.9926	0.9948
1.0	0.9864	0.9897
1.5	0.9802	0.9848
2.0	0.9745	0.9801
2.5	0.9692	0.9756
3.0	0.9645	0.9713
3.5	0.9601	0.9671
4.0	0.9562	0.9631
4.5	0.9528	0.9593

This implies that ultrasonic data gathered up to 1.5 GPa predicts the compression of SiC/Al to at least 4.5 GPa. These results point out that while dilation measurements provide accurate compression for a solid, material constants like bulk modulus and pressure derivative of bulk modulus cannot be reliably obtained from these measurements. For example, the values of bulk modulus and pressure derivative of the bulk modulus of SiC/Al obtained from ultrasonic measurements are 94.1 GPa and 5.21, respectively. The values of these parameters from Equation 13 are 68.8 GPa and 7.5. It should be noted that this value of bulk modulus, i.e., 68.8 GPa for SiC/Al, is less than the value of the bulk modulus of a more compressible component of SiC/Al; i.e., 2014-T4 aluminum which is 77.2 GPa.

Conclusions

The conclusions that may be drawn from this work are:

1. Compression of a composite can be obtained by dilational measurements made in a piston cylinder apparatus, and by the method used in this report to calculate the volume change of the composite with pressure.

2. SiC/Al, the material investigated in this report, appears to be isotropic.

3. The compression equations given by Equations 29 and 30 yield the values of ratios of volumes up to 4.5 GPa within 0.7% of each other.

SHOCK RESPONSE

Introduction

One of the properties of interest from the point of view of vulnerability under impact condition is to determine response, or deformation, of the material under shock loading. This section gives the results of a limited number of shock compression experiments performed on SiC/2014-T4 Al of two orientations to 5.2 GPa. The two orientations of SiC/2014-T4 Al result from the fabrication process of this composite described in the Materials Description Section. The results of this section, even though based on a limited number of experiments, do provide some pertinent, but preliminary, information regarding both the nature of the deformation of this composite under shock compression and its spall threshold.

Specimen and Experimental Details

Specimens of SiC/2014-T4 Al used in the shock wave experiments were circular discs with 31.75-mm diameter and thickness varying between 2 mm and 8 mm. The specimens were flat to 5 micron and opposing faces of the discs were mutually parallel within 0.4 parts per thousand over their lateral dimensions.

The shock experiments were performed with a 10.2-cm-diameter light gas gun facility at the U.S. Army Materials Technology Laboratory. Direct impact and transmission shock experiments were performed to determine the Hugoniot of SiC/2014-T4 Al to 5.2 GPa. In addition, tension-inducing shock wave experiments were conducted to determine the spall threshold in SiC/2014-T4 Al. The details of direct impact and transmission experiments and

the procedure for the reduction of experimental data to deduce the shock compressed state of the material of interest can be found in Ref. 28 and 29. In every spall experiment, a 2-mm-thick disc of SiC/2014-T4 Al impacted a 4-mm disc of SiC/2014-T4 Al. Existence, or absence, of spall in the composite was inferred by examining the sliced discs of SiC/2014-T4 Al recovered in these experiments under microscope. All experiments were conducted in vacuum pressure of less than 7 GPa.

The parameters measured in the direct impact and transmission experiments were impact velocity and stress profile, as recorded by an X-cut quartz gage. The X-cut quartz gages were either used in shunted or shorted mode according to the prescription suggested by Graham.[30] The uncertainties in the measurements of impact velocity and stress by X-cut quartz gages were 0.5% and 2.5%, respectively. During the spall experiments, only the impact velocities were measured. The planarity of the impact in the experiments of the present investigation never deviated by more than 2 mrad.

Results

The results of direct impact and transmission experiments are given in Tables 7 and 8. Figure 28 provides a graphic representation of stress (σ) versus particle velocity (u) of SiC/Al (z) and SiC/Al (r). Table 8 shows that the HEL values of SiC/Al (z) and SiC/Al (r) vary between 0.3 GPa and 0.335 GPa, and 0.275 GPa and 0.368 GPa, respectively. Calculation of the magnitude of HEL (σ_{HEL}) estimated from the static proportional elastic limit (Y_0) data on SiC/2014-T4 Al from the relation

$$\sigma_{HEL} = [\ (1 - \nu)\ /\ (1 - 2\nu)\ ]Y_0 \qquad (31)$$

yields a value of 0.398 ± 0.113 GPa. In the above relation, the value of Y_0 has been found to be 0.225 ± 0.064 GPa for SiC/2014-T4 Al,[31] ν is the Poisson's ratio and has a value of 0.303, as obtained from the elastic wave velocities for SiC/2014-T4 Al given earlier. The values of HEL obtained in these shock experiments appear to be lower than the estimates of HEL obtained from the static proportional elastic limit data. One possible reason for this discrepancy may lie in the fact that the stress strain for SiC/Al (z) and SiC/Al (r) did not show a sharp yield stress like in 2014 aluminum alloy. The wave profiles obtained in the transmission experiments listed in Table 2 do not show any elastic precursor decay in 6-mm- to 8-mm-thick specimens of SiC/Al (z) or SiC/Al (r). Thus, the values of HEL may be taken as the range of HEL for SiC/2014-T4 Al, and the scatter in the HEL values are probably real and, thus, indicative of material variability.

28. LYSNE, P. C., PERCIVAL, C. M., BOADE, R. R., and JONES, O. E. *Determination of Release Adiabats and Recentered Hugoniot Curves by Shock Reverberation Techniques.* J. Appl. Phys., v. 40, no. 3786, 1969.
29. DANDEKAR, D. P., MARTIN, A. G., and KELLEY, J. V. *Deformation of Depleted Uranium 0.78 Ti Under Shock Compression to 11.0 GPa at Room Temperature.* J. Appl. Phys., v. 51, no. 4784, 1980.
30. GRAHAM, R. A. *Piezoelectric Current from Shunted and Shorted Guard-Ring Quartz Gauges.* J. Appl. Phys., v. 46, no. 1901, 1975.
31. CHOU, S. C., GREEN, J. L., and SWANSON, R. A. *Mechanical Behavior of Silicon Carbide/2014 Aluminum Composite.* Testing Technology of Metal Matrix Composites, ASTM STP 964, P. R. D. Giovanni and N. R. Adsit, ed., American Society for Testing and Materials, Philadelphia, PA, 1988, p. 305-316.

Table 7. SUMMARY OF DIRECT IMPACT EXPERIMENTS IN SiC/2014-T4 ALUMINUM

Experiment	Buffer	Final Compression: Impact Velocity (km/sec)	Stress (GPa)	Particle Velocity (km/sec)	Final Shock Velocity* (km/sec)
SiC/Al (z)					
8410	WC	0.361	5.18	0.311	5.64
8418	Sapphire	0.348	4.05	0.255	5.34
SiC/Al (r)					
8504	None	0.206	1.7	0.094	6.00

*These velocities were determined assuming a HEL of 0.314 GPa

Table 8. SUMMARY OF TRANSMISSION EXPERIMENTS IN SiC/2014-T4 ALUMINUM

			Elastic Compression				Final Compression			
Experiment	Specimen Thickness (mm)	Impactor	Impact Velocity (km/sec)	Stress (GPa)	Particle Velocity (km/sec)	Density (Mg/m^3)	Impact Velocity (km/sec)	Stress (GPa)	Particle Velocity (km/sec)	Density (Mg/m^3)
SiC/Al (z)										
8410	8.00	SiC/Al (z)	0.361	0.335	0.0158	2.912	5.33	2.89	0.181	3.02
8509	7.78	SiC/Al (z)	0.256	0.311	0.0150	2.912	5.05	1.96	0.128	2.97
8518	7.89	SiC/Al (z)	0.204	0.300	0.0141	2.912	5.02	1.58	0.102	2.96
SiC/Al (r)										
8504	7.452	SiC/Al (r)	0.206	0.275	0.013	2.911	5.92	1.82	0.103	2.96
8522	7.920	2014-T4 Al	0.167	0.296	0.014	2.912	5.9	1.34	0.0747	2.94
8522	6.300	2014-T4 Al	0.167	0.368	0.0173	2.913	5.8	1.27	0.071	2.94

The deformation of SiC/2014-T4 Al above the HEL presented in terms of (σ, u) coordinates (Figure 29) appear to be consistent with each other irrespective of whether these coordinates were obtained from direct impact or from transmission experiments for each z and r oriented specimens. However, the nonelastic deformation of SiC/Al (z) and SiC/Al (r) differ in regard to the estimates of shock velocities following the elastic precursors in these specimens. The estimates of final shock velocities in SiC/Al (z) are consistently lower than the estimates of these velocities in SiC/Al (r) and the bulk sound speed of 5.76 ± 0.03 km/sec in SiC/2014-T4 Al. The reason for this consistent difference in the estimates of final shock velocities in SiC/Al (z) and SiC/Al (r) is unknown. The deformation behavior of SiC/Al (z) and SiC/Al (r) above the HEL will be investigated in further detail in the future.

There appears to be some difference in the spall thresholds of SiC/Al (z) and SiC/Al (r) as indicated in Table 9. It shows that whereas SiC/Al (z) spalls when it is impacted by itself with a velocity of 0.153 km/sec, SiC/Al (r) does not spall when impacted with similar velocity. However, a definite conclusion about the implied difference in the spall threshold of SiC/Al (z) and SiC/Al (r) must await performance of more spall experiments.

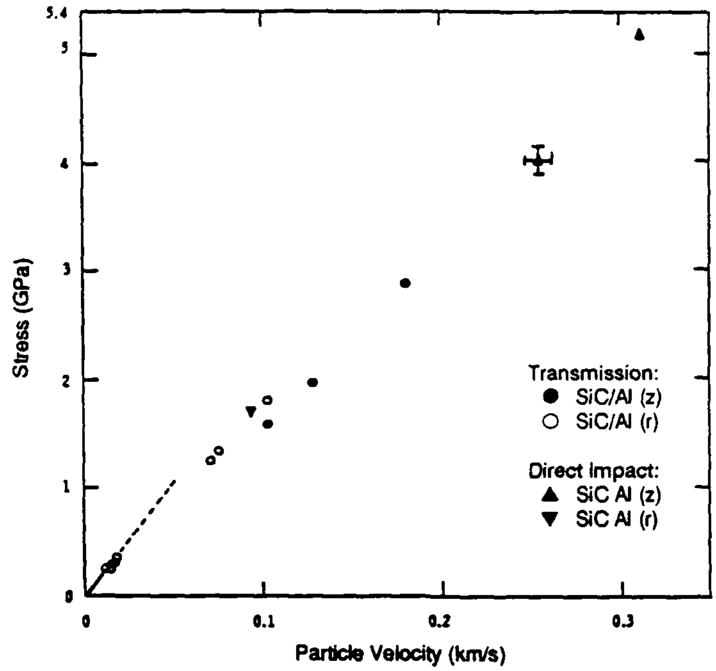

Figure 29. Stress-particle velocity diagram of SiC/Al (z) and SiC/Al (r).

Table 9. SUMMARY OF SPALL EXPERIMENTS ON SiC/2014-T4 ALUMINUM

Experiment	Impact Velocity (km/sec)	Spall
SiC/Al (z)		
8425	0.153	Yes
8501	0.133	No
SiC/Al (r)		
8501	0.133	No
8506	0.151	No
8508	0.191	Yes
8520	0.175	Yes

SUMMARY

Density

The measured density of SiC/Al was not found to be significantly different from the theoretical density of the composite and, hence, can be 2.906 ± 0.02 Mg/m^3.

Elastic Constants

The values of elastic constants determined from the ultrasonic velocity measurements and stress-strain curve measurements are given in Table 10. It is obvious that these sets of

measurements are consistent with each other, and one can safely use these values for the purpose of calculating elastic deformation under different load conditions, but below the yield stress value.

Table 10. VALUES OF ELASTIC CONSTANTS OF SiC/2014-T4 Al AT THE AMBIENT CONDITION

Elastic Constants	Units	Ultrasonic	Stress-Strain
Young's	GPa	114 ± 2	121
Shear	GPa	43.8 ± 0.7	44.8
Poisson's Ratio	GPa	0.303 ± 0.006	0.3

The pressure dependence of the bulk modulus of SiC/2014-T4 Al is determined to be 5.42 larger than the pressure dependence of the moduli of its constituents. However, the pressure dependence of the shear modulus is comparable to those of its constituents. This implies that under pressure, SiC/2014-T4 Al becomes relatively more stiff than either of its constituents; i.e., dimensional stability is enhanced under pressure. The proportional increase in shear modulus is comparable to that of its constituents at high pressure.

The temperature dependence of the Young's modulus is determined to be 7.59×10^{-2} GPa/°C to 540°C; i.e., the value of Young's modulus of SiC/2014-T4 Al at 540°C is 80 GPa higher than the value of Young's modulus of 2014-T4 at room temperature. In other words, it will be advantageous to use this composite instead of 2014/T4 aluminum in a situation where temperature is too high for aluminum to sustain.

Limits of Elastic Deformation, Ductility, and Strength

SiC/2014-T4 Al was found to be strain-rate insensitive, both under compression as well as tension. The value of yield stress was determined to be 260 MPa.

Ductility of SiC/2014-T4 Al is considerably reduced compared to 2014-T4 Al. The strains of failure for the composite at room temperature, and at 540°C, were found to be 1.5% and 2.5%, respectively. The said reduction in ductility was also evident from the observed maximum twist angle per unit length of around 1.57°C/mm.

The ultimate strength of SiC/2014-T4 Al was found to be 586 MPa at room temperature. The ultimate strength of the composite at 540°C, when the heating rates were 250°C/sec and 28°C/sec, were found to be around 225 MPa and 125 MPa, respectively; much larger than that of 2014-T4 Al under similar conditions.

The results of Bauschinger effect in SiC/2014-T4 Al indicated that the material possesses a fixed total available tensile strain of approximately 1.5% which was not affected by the two precompression levels of 1% and 2%. Also, it failed at approximately 586 MPa, just as in the monotonic tension tests.

The average value of K_{Ic} was found to be 13.3 MPa to 13.7 MPa, lower than the K_{Ic} value for 2014-T6 Al; i.e., 19.3 MPa.

Equation of State

The isothermal and adiabatic volumetric compressions of SiC/2014-T4 Al can be represented by the following two relations:

$$V(P)/V(0) = 1 - 1.454 \times 10^{-2}P + 8.9815 \times 10^{-4}P^2$$

and

$$V(P)/V(0) = 1 - 1.0341 \times 10^{-4}P + 3.4323 \times 10^{-4}P^2.$$

Shock Deformation

The value of the Hugoniot Elastic Limit, i.e., limit of elastic deformation of SiC/2014-T4 Al, was determined to be 0.32 ± 0.05 GPa.

The spall thresholds of SiC/Al (z) and SiC/Al (r) were found to be 1.52 GPa, and 1.0 GPa, respectively. This appears to be the only parameter of this material dependent on its orientation.

The deformation behaviors of SiC/Al (z) and SiC/Al (r) above HEL show a puzzling behavior; namely, the shock velocities in SiC/Al (z) are consistently lower than in SiC/Al (r) and lower than the bulk sound speed of 5.76 km/sec. This aspect needs to be investigated further before any conclusion regarding the nature of deformation of SiC/Al above its HEL can be definitively made.

REFERENCES

1. BARKER, L. M. *Theory for Determining K_{Ic} from Small Non-LEFM Specimens, Supported by Experiments on Aluminum.* International Journal of Fracture, v. 15, no. 6, December 1979, p. 515-536.
2. Fractometer System 4202 Owner's Manual. Terra Tek, Inc., Salt Lake City, Utah, 1983.
3. HILL, R. *The Mathematical Theory of Plasticity.* Oxford University Press, New York, 1950.
4. MIL-HDBK-5D. *Typical Values of Room Temperature Plane-Strain Fracture Toughness of Aluminum Alloys.* 1 June 1983, p. 3-11.
5. SMYTHE, W. R. *Static and Dynamic Electricity, Third Edition.* McGraw-Hill, New York, 1968.
6. MARION, R. H. *A New Method of High-Temperature Strain Measurement.* Experimental Mechanics, v. 18, no. 4, April 1978, p. 134-140.
7. Aerospace Structural Metals Handbook. v. 3, 1979, p. 25.
8. HASHIN, Z., and SHTRIKMAN, S. *A Variational Approach to the Theory of the Elastic Behaviour of Multiphase Materials.* J. Mechanics and Physics of Solids, v. 11, 1963, p. 127-140.
9. MAEWAL, A., and DANDEKAR, D. P. *Effective Thermoelastic Properties of Short-Fiber Composites.* Acta. Mech., v. 66, 1987, p. 191-204.
10. MORI, T., and TANAKA, K. *Average Stress in Matrix and Average Elastic Energy of Materials with Misfitting Inclusions.* Acta. Metallurgica, v. 21, 1973, p. 571-574.
11. TAYA, M., and CHOU, T. W. *On Two Kinds of Ellipsoidal Inhomogeneities in an Infinite Elastic Body: An Application to a Hybrid Composite.* International Journal of Solids and Structures, v. 17, 1981, p. 553-565.
12. WENG, G. J. *Some Elastic Properties of Reinforced Solids, with Special Reference to Isotropic Ones Containing Spherical Inclusions.* International Journal of Engineering Science, v. 22, 1984, p. 845-856.
13. TANDON, G. P., and WENG, G. J. *The Effect of Aspect Ratio of Inclusions on the Elastic Properties of Unidirectionally Aligned Composites.* Polymer Composites, v. 5, 1984, p. 327-333.
14. PAPADAKIS, E. P. *Ultrasonic Phase Velocity by the Pulse-Echo-Overlap Method Incorporating Diffraction Phase Corrections.* Journal of the Acoustical Society of America, v. 42, 1967, p. 1045-1051.
15. SCHREIBER, E., and SOGA, N. *Elastic Constants of Silicon Carbide.* Journal of the American Ceramic Society, v. 49, 1966, p. 342.
16. BABCOCK, S. G., LANGAN, J. J., NORVEY, D. B., MICHAELS, T. E., SCHIERLOH, F. L., and GREEN, S. G. *Characterization of Three Aluminum Alloys.* U.S. Army Materials Technology Laboratory, AMMRC CR 71-3, January 1971.
17. DANDEKAR, D. R. *Iterative Procedure to Estimate the Values of Elastic Constants of a Cubic Solid at High Pressures from the Sound Wave Velocity Measurements.* Journal of Applied Physics, v. 41, 1970, p. 667-672.
18. GUBBAY, J. D. *Micromechanical Properties of Al/SiC Metal Matrix Composite.* The Charles Stark Draper Laboratory Final Reports CSDL-R-1578, The Charles Stark Draper Laboratory, Inc., Cambridge, MA, June 1982.
19. CHRISTENSEN, R. M. *Mechanics of Composite Materials.* John Wiley and Sons, New York, 1979, p. 311-339.
20. McQUEEN, R. J., MARSH, S. P., TAYLOR, J. W., FRITZ, J. N., and CARTER, W. J. in *High Velocity Impact Phenomena.* Ray Kinslow, ed., Chapter VII and Appendix E, Academic Press, New York, 1970, p. 293-417 and p. 549.
21. GUST, W. H., HOLT, A. C., and ROYCE, E. B. *Dynamic Yield, Compressional, and Elastic Parameters for Several Lightweight Intermetallic Compounds.* Journal of Applied Physics, v. 44, 1973, p. 550-560.
22. FOWLES, G. R. *Shock Wave Compression of Hardened and Annealed 2024 Aluminum.* Journal of Applied Physics, v. 32, 1961, p. 1475-1487.
23. STEINBERG, D. J. *Equations of State for the Ceramics BeO and B C.* UCID-16946, Lawrence Livermore National Laboratory, Livermore, CA, November 1975.
24. MAUER, F. A., MUNRO, R. G., PIERMARINI, G. J., BLOCK, S., and DANDEKAR, D. P. *Compression Studies of a Nickel-Based Superalloy, MAR-M200, and of Ni_3Al.* J. Appl. Phys., v. 58, no. 3727, 1985.
25. DANDEKAR, D. P., FRANKEL, J., and KORMAN, W. J. *Pressure Dependence of the Elastic Constants of Silicon Carbide/2014 Aluminum Composite.* Testing Technology of Metal Matrix Composites, ASTM STP 964, P. R. DiGiovanni and N. R. Adsit, ed., American Society for Testing and Materials, Philadelphia, PA, 1988, p. 79-89.
26. VAIDYA, S. N., and KENNEDY, G. C. *Compressibility of 18 Metals to 45 kbar.* J. Phys. Chem. Solids, v. 31, no. 2329, 1970.
27. SINGH, A. K., and KENNEDY, G. C. *Compression of Calcite to 40 kBar.* J. Geophys. Res., v. 79, no. 2615, 1974.
28. LYSNE, P. C., PERCIVAL, C. M., BOADE, R. R., and JONES, O. E. *Determination of Release Adiabats and Recentered Hugoniot Curves by Shock Reverberation Techniques.* J. Appl. Phys., v. 40, no. 3786, 1969.
29. DANDEKAR, D. P., MARTIN, A. G., and KELLEY, J. V. *Deformation of Depleted Uranium 0.78 Ti Under Shock Compression to 11.0 GPa at Room Temperature.* J. Appl. Phys., v. 51, no. 4784, 1980.
30. GRAHAM, R. A. *Piezoelectric Current from Shunted and Shorted Guard-Ring Quartz Gauges.* J. Appl. Phys., v. 46, no. 1901, 1975.
31. CHOU, S. C., GREEN, J. L., and SWANSON, R. A. *Mechanical Behavior of Silicon Carbide/2014 Aluminum Composite.* Testing Technology of Metal Matrix Composites, ASTM STP 964, P. R. D. Giovanni and N. R. Adsit, ed., American Society for Testing and Materials, Philadelphia, PA, 1988, p. 305-316.

DISTRIBUTION LIST

No. of Copies	To
	Office of Deputy Under Secretary of Defense for Research and Engineering, The Pentagon, Washington, DC 20301
1	ATTN: J. Persh, Staff Specialist for Materials and Structures (Room 3D1089)
	Office of Deputy Chief of Research, Development and Acquisition, The Pentagon, Washington, DC 20301
1	ATTN: DAMA-CSS
	Commander, U.S. Army Laboratory Command, 2800 Powder Mill Road, Adelphi, MD 20783-1145
1	ATTN: AMSLC-TD, Office of the Technical Director
	Commander, U.S. Army Materiel Command, 5001 Eisenhower Avenue, Alexandria, VA 22333-0001
1	ATTN: AMCLD
1	AMCSCI, Dr. Chait (Room 10E20)
	Strategic Defense Initiative Office, The Pentagon, Washington, DC 20304
1	ATTN: SLKT, Major R. Yesensky
1	SLKT, A. Young
	Director, U.S. Strategic Defense Command, P.O. Box 1500, Huntsville, AL 35807-3801
1	ATTN: CSSD-H-QX, D. Bouska
1	CSSD-H-LK, L. Atha
1	CSSD-H-LK, L. Cochran
1	CSSD-H-HA, R. Buckelew
1	CSSD-H-E, J. Katechis
1	CSSD-H-Q, E. Wilkinson
1	CSSD-H-Q, R. Riviera
1	CSSD-H-QE, J. Papadopoulos
	Commander, U.S. Army Missile Command, Redstone Arsenal, Huntsville, AL 35809
1	ATTN: AMSMI-EAM, P. Ormsby
	Commander, U.S. Army Combat Development Command, Institute of Nuclear Studies, Fort Bliss, TX 79916
1	ATTN: Technical Library
	Commander, Naval Surface Warfare Center, Silver Springs, MD 20910
1	ATTN: J. Foltz
	Commander, U.S. Air Force Wright Aeronautical Laboratories, Wright-Patterson Air Force Base, OH 45433
1	ATTN: AFWAL/FIBAA, A. Gunderson
1	AFWAL/FIBAA, C. R. Waitz
1	AFWAL/MLLS, T. Ronald

No. of Copies	To
	Commander, BMO/ASMS, Norton Air Force Base, CA 92409
1	ATTN: Capt. T. Williams
	Director, Defense Nuclear Agency, Washington, DC 20305-1000
1	ATTN: B. Gillis
	Commander, Defense Technical Information Center, Cameron Station, Building 5, 5010 Duke Street, Alexandria, VA 22304-6145
2	ATTN: DTIC-FDAC
	National Aeronautics and Space Administration, Langley Research Center, Hampton, VA 23665
1	ATTN: W. Brewer, Code MS-224
	Institute for Defense Analysis, 1801 N. Beauregard Street, Alexandria, VA 22311
1	ATTN: M. Rigdon
	Aerospace Corporation, P.O. Box 92957, Los Angeles, CA 90009
1	ATTN: L. McCreight
1	H. Katzman
	AVCO Systems Division of Textron, Inc., 201 Lowell Street, Wilmington, MA 01887
1	ATTN: V. DiCristina
	AVCO Specialty Materials, Subsidiary of Textron, Inc., 2 Industrial Avenue, Lowell, MA 01851
1	ATTN: P. Hoffman
1	M. Mittnick
	The Boeing Aerospace Company, P.O. Box 3999, Seattle, WA 98124
1	ATTN: S. Bigelow
1	P. G. Rimbos
1	B. K. Das
1	T. Luhman
	Charles Stark Draper Laboratories, 555 Technology Avenue, Cambridge, MA 02139
1	ATTN: J. Gubbay
	DWA Composite Specialties, Inc., 21133 Superior Street, Chatsworth, CA 91311
1	ATTN: J. F. Dolowy, Jr.
	Fiber Materials, Inc., Biddeford Industrial Park, Biddeford, ME 04005
1	ATTN: R. Burns
	General Dynamics Corporation, Convair Division, P.O. Box 80847, San Diego, CA 92130
1	ATTN: J. Hertz
1	K. Meyer

No. of Copies	To
	General Electric Company, Advanced Materials Development Laboratory, 3198 Chestnut Street, Philadelphia, PA 19101
1	ATTN: J. Brazel
1	K. Hall
	General Electric Company, Valley Forge Space Center, P.O. Box 8555, Philadelphia, PA 19101
1	ATTN: C. Zweben
	General Research Corporation, P.O. Box 6770, 5383 Hollister Avenue, Santa Barbara, CA 93111
1	ATTN: J. Green
	Kaman Tempo, 816 State Street, Santa Barbara, CA 93101
1	ATTN: L. Gonzalez
	Lockheed-Georgia Company, 86 South Cobb Drive, Marietta, GA 30063
1	ATTN: J. Carrol
1	W. Bates
	Lockheed Missile and Space Company, 1111 Lockheed Way, Sunnyvale, CA 94089
1	ATTN: W. Loomis
1	D. Himmelblau
1	R. Torczyner
1	H. Chang
	Martin Marietta Orlando Aerospace, P.O. Box 5837, Orlando, FL 32085
1	ATTN: R. Caime
1	K. Hanson
1	F. Koo
1	M. Hendricks
	Martin Marietta Baltimore Aerospace, 103 Chesapeake Park Plaza, Baltimore, MD 21220
1	ATTN: W. Couch
	Martin Marietta Denver Aerospace, P.O. Box 179, Denver, CO 80201
1	ATTN: M. Misra
	Material Concepts, Inc., 666 North Hague Avenue, Columbus, OH 43204
1	ATTN: D. Kizer
	McDonnell Douglas Astronautics Company, 5301 Bolsa Avenue, Huntington Beach, CA 92647
1	ATTN: J. Ditto
1	J. Davidson
1	J. Grossman
1	H. Parachanian
1	B. Leonard

No. of Copies	To
	PDA Engineering, 2975 Red Hill Avenue, Costa Mesa, CA 92626
1	ATTN: M. Sherman
	Rohr Industries, Inc., Foot of H Street, P.O. Box 878, Chula Vista, CA 92012-0878
1	ATTN: N. R. Adsit
	SPARTA, Inc., 1055 Wall Street, Suite 200, P.O. Box 1354, La Jolla, CA 92038
1	ATTN: J. Glatz
1	G. Wonacott
	SPARTA, Inc., 3440 Carson Street, Suite 300, Torrance, CA 90503
1	ATTN: I. Osofsky
	SPARTA, Inc., 1104B Camino Del Mar, Del Mar, CA 92014
1	ATTN: D. Weisinger
	Southwest Research Institute, 8500 Culebra Road, San Antonio, TX 78206
1	ATTN: A. Wenzel
	Stone Engineering Company, 805 Madison Street, Suite 2C, Huntsville, AL 35801
1	ATTN: W. Stone
	Teledyne Brown Engineering, Research Park, 300 Sparkman Drive, Huntsville, AL 35807
1	ATTN: C. Patty
	Director, U.S. Army Materials Technology Laboratory, Watertown, MA 02172-0001
1	ATTN: SLCMT-TML
8	Authors

U.S. Army Materials Technology Laboratory
Watertown, Massachusetts 02172-0001
DEFORMATION BEHAVIOR OF SiC/2014 Al
METAL-MATRIX COMPOSITE -
Shun-Chin Chou, Dattatraya P. Dandekar,
Julius Frankel, Jibmitra Ganguly, John L. Green,
Craig Lopatin, Anthony G. Martin, and
Ronald Swanson

AD___________
UNCLASSIFIED
UNLIMITED DISTRIBUTION

Key Words

Elastic constants
High temperature
Spallation

Technical Report MTL TR 89-42, May 1989, 46 pp-
illus-tables, D/A Project: 536-6010 P623222.K14A-2585
AMCMS Code: 69200R.897 A050

The deformation behavior of a composite composed of 25-volume-percent silicon carbide (SiC) whiskers in 2014 aluminum matrix was studied. Specimens were taken from a hot isostatically pressed cylindrical billet, then tested at various loading conditions and strain rates. Mechanical deformation of the composite was performed using tension, compression, torsion, Bauschinger effect, and fracture toughness testing. Deformation of the composite under shock loading/unloading and spallation threshold were determined. Elastic wave velocities at high pressures to 1.5 GPa and volume compression to 4.5 GPa were measured to determine the pressure dependence of elastic constants and isothermal and adiabatic equations of state.

U.S. Army Materials Technology Laboratory
Watertown, Massachusetts 02172-0001
DEFORMATION BEHAVIOR OF SiC/2014 Al
METAL-MATRIX COMPOSITE -
Shun-Chin Chou, Dattatraya P. Dandekar,
Julius Frankel, Jibmitra Ganguly, John L. Green,
Craig Lopatin, Anthony G. Martin, and
Ronald Swanson

AD___________
UNCLASSIFIED
UNLIMITED DISTRIBUTION

Key Words

Elastic constants
High temperature
Spallation

Technical Report MTL TR 89-42, May 1989, 46 pp-
illus-tables, D/A Project: 536-6010 P623222.K14A-2585
AMCMS Code: 69200R.897 A050

The deformation behavior of a composite composed of 25-volume-percent silicon carbide (SiC) whiskers in 2014 aluminum matrix was studied. Specimens were taken from a hot isostatically pressed cylindrical billet, then tested at various loading conditions and strain rates. Mechanical deformation of the composite was performed using tension, compression, torsion, Bauschinger effect, and fracture toughness testing. Deformation of the composite under shock loading/unloading and spallation threshold were determined. Elastic wave velocities at high pressures to 1.5 GPa and volume compression to 4.5 GPa were measured to determine the pressure dependence of elastic constants and isothermal and adiabatic equations of state.

U.S. Army Materials Technology Laboratory
Watertown, Massachusetts 02172-0001
DEFORMATION BEHAVIOR OF SiC/2014 Al
METAL-MATRIX COMPOSITE -
Shun-Chin Chou, Dattatraya P. Dandekar,
Julius Frankel, Jibmitra Ganguly, John L. Green,
Craig Lopatin, Anthony G. Martin, and
Ronald Swanson

AD___________
UNCLASSIFIED
UNLIMITED DISTRIBUTION

Key Words

Elastic constants
High temperature
Spallation

Technical Report MTL TR 89-42, May 1989, 46 pp-
illus-tables, D/A Project: 536-6010 P623222.K14A-2585
AMCMS Code: 69200R.897 A050

The deformation behavior of a composite composed of 25-volume-percent silicon carbide (SiC) whiskers in 2014 aluminum matrix was studied. Specimens were taken from a hot isostatically pressed cylindrical billet, then tested at various loading conditions and strain rates. Mechanical deformation of the composite was performed using tension, compression, torsion, Bauschinger effect, and fracture toughness testing. Deformation of the composite under shock loading/unloading and spallation threshold were determined. Elastic wave velocities at high pressures to 1.5 GPa and volume compression to 4.5 GPa were measured to determine the pressure dependence of elastic constants and isothermal and adiabatic equations of state.

U.S. Army Materials Technology Laboratory
Watertown, Massachusetts 02172-0001
DEFORMATION BEHAVIOR OF SiC/2014 Al
METAL-MATRIX COMPOSITE -
Shun-Chin Chou, Dattatraya P. Dandekar,
Julius Frankel, Jibmitra Ganguly, John L. Green,
Craig Lopatin, Anthony G. Martin, and
Ronald Swanson

AD___________
UNCLASSIFIED
UNLIMITED DISTRIBUTION

Key Words

Elastic constants
High temperature
Spallation

Technical Report MTL TR 89-42, May 1989, 46 pp-
illus-tables, D/A Project: 536-6010 P623222.K14A-2585
AMCMS Code: 69200R.897 A050

The deformation behavior of a composite composed of 25-volume-percent silicon carbide (SiC) whiskers in 2014 aluminum matrix was studied. Specimens were taken from a hot isostatically pressed cylindrical billet, then tested at various loading conditions and strain rates. Mechanical deformation of the composite was performed using tension, compression, torsion, Bauschinger effect, and fracture toughness testing. Deformation of the composite under shock loading/unloading and spallation threshold were determined. Elastic wave velocities at high pressures to 1.5 GPa and volume compression to 4.5 GPa were measured to determine the pressure dependence of elastic constants and isothermal and adiabatic equations of state.